Interaction Notes

Note 85

8 November 1971

Induced Electric Currents on Some Configurations of Wires

Part I.
Perpendicular Crossed Wires

Clayborne D. Taylor
Terry T. Crow
Mississippi State University
State College, Mississippi 39762

Induced Electric Currents on Some Configurations of Wires

Part I.
Perpendicular Crossed Wires

ABSTRACT

The development of a system of integral equations for a system of thin conducting wires in an arbitrary geometry is outlined. These equations are then applied to a set of two perpendicular intersecting wires.

FOREWORD

For convenience the figures used in the development of the theory are included in the text. Figures showing results of the parameter study are grouped together at the end of the report. We should like to thank Dr. Carl Baum and Capt. P. R. Barnes for helpful suggestions and discussions concerning this work. To Mr. T. H. Shumpert and Mr. B. D. Graves we express our appreciation for their help in the numerical calculations and preparation of the final report.

1. Introduction

The theoretical study of certain classes of electromagnetic problems has become feasible with the development of high speed computing techniques. Various forms of integral equations have been developed for the study of electric currents induced on arbitrary configurations of thin conducting wires by incident electric fields. The development of one such set--Hallen's--is outlined here and follows work previously reported [1,2]. In general, an N-wire system will have N coupled integral equations associated with it, and, if the wires physically intersect, there will be two additional constraints; the continuity of the scalar potential at the junctions and the Kirchhoff current law.

2. The Integral Equations

The well-known equations for the tangential component of the vector potential and the scalar potential at a point S on the conductor are

$$A_S(S) = \frac{\mu_o}{4\pi} \int_L I(S')\ \hat{S}'\cdot\hat{S}\ G(S,S')\ dS' \tag{1}$$

$$\phi(S) = \frac{1}{4\pi\varepsilon_o} \int_L \lambda(S')\ G(S,S')\ dS' \tag{2}$$

where $G(S,S')$ is the usual Green's function and $I(S')$ and $\lambda(S')$ the linear current and charge densities, respectively. With the equation of continuity and an assumed harmonic time dependence, frequency ω, the ϕ equation becomes

$$\phi(S) = \frac{j\zeta}{4\pi k} \int \frac{dI(S')}{dS'} \; G(S,S') \; dS' \tag{3}$$

For an N wire system, the scalar potential on the n^{th} wire becomes

$$\phi_n(S_n) = \frac{j\zeta}{4\pi k} \sum_{m=1}^{N} \int dS'_m \; G(S_n,S'_m) \; \frac{d\, I(S'_m)}{d\, S'_m} \tag{4}$$

The tangential component of the total electric field at the surface of the conductor is set equal to zero, i.e.

$$E_{S_n} \; (S_n) + E^i_{S_n} \; (S_n) = 0 \tag{5}$$

where $E^i_{S_n} \; (S_n)$ is the incident field and $E_{S_n} \; (S_n)$ is the scattered field. The E field in terms of ϕ and $\vec{A}$ becomes

$$-E^i_{S_n} \; (S_n) = - \frac{d}{dS_n} \; \phi_n(S_n) - j\omega \; A_{S_n} \; (S_n) \tag{6}$$

The definition of $\Phi_n(S_n)$ as

$$\Phi_n(S_n) = -j \; \frac{k^2}{\omega} \int_0^{S_n} dS'_n \; \phi_n(S'_n) \tag{7}$$

allows one to work with a set of integral equations (rather than integro-differential equations) and in the form

$$\frac{d^2\Phi_n}{d\, S_n^2} + k^2\Phi_n = k^2 \left[\Phi_n - A_{S_n} \; (S_n)\right] - j \; \frac{k^2}{\omega} \; E^i_{S_n} \; (S_n) \tag{8}$$

The formal solution of (8) is

$$\Phi_n(S_n) = C_n \cos k\, S_n + D_n \sin kS_n$$

$$+ k \int_0^{S_n} d\, S_n' \left[\Phi_n(S_n') - A_{S_n}(S_n')\right] \sin k(S_n - S_n')$$

$$- j \frac{k}{\omega} \int_0^{S_n} dS_n'\, E^i_{S_n}(S_n') \sin k(S_n - S_n') \qquad (9)$$

The integral equations resulting from (9) are

$$\sum_m \int_{L_m} d\, S_m'\, I_m(S_m')\, \Pi(S_n, S_m') = C_n' \cos k\, S_n + D_n' \sin k\, S_n$$

$$- j \frac{4\pi}{\zeta} \int_0^{S_n} d\, S_n'\, E^i_{S_n}(S_n') \sin k(S_n - S_n') \qquad (10)$$

In this derivation it is assumed that the wires have free ends such that $I_m(0) = I_m(L_m) = 0$. The Π term is

$$\Pi(S_n, S_m') = (\hat{S}_m' \cdot \hat{S}_n)\, G(S_n, S_m') - \int_0^{S_n} d\, S_n' \cos k(S_n - S_n')\, \Psi(S_n', S_m') \qquad (11)$$

and

$$\Psi(S_n', S_m') = \frac{\partial G(S_n', S_m')}{\partial S_m'} + G(S_n', S_m') \frac{\partial}{\partial S_n'} (\hat{S}_m \cdot \hat{S}_n')$$

$$+ (\hat{S}_m' \cdot \hat{S}_n') \frac{\partial}{\partial S_n'} G(S_n', S_m') \qquad (12)$$

The N-wire system to be considered is one in which there is a single common intersection point. This point of intersection is chosen to be the origin of the coordinate system. The two boundary conditions become

$$\lim_{\delta \to 0} \sum_{n=1}^{N} \left[I_n (+\delta) - I_n (-\delta) \right] = 0 \tag{13}$$

$$\phi_1(0) = \phi_n(0) \qquad n = (2, ---, N) \tag{14}$$

From equations (7) and (9), the ϕ boundary condition implies

$$D_1 = D_n \qquad (n = 2, ---, N) \tag{15}$$

3. The Two Wire System

The integral equations (10) are now applied to a two wire system aligned as shown in Figure 1, where wire 1 refers to that along the y-axis and wire 2 to that along the x-axis.

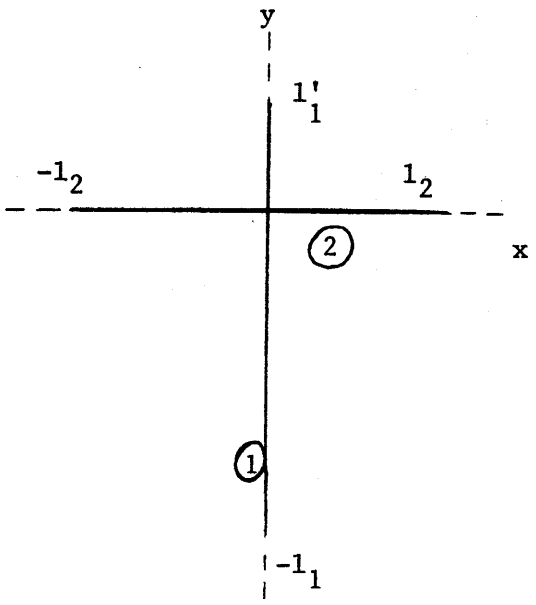

Figure 1

For this system

$$\int_{-l_1}^{l_1'} dy'\, I_1(y')\, \Pi(y,y') + \int_{-l_2}^{l_2} dx'\, I_2(x')\, \Pi(y,x')$$

$$= C_1 \cos k y + D_1 \sin k y - j \frac{4\pi}{\zeta} \int_0^y dy'\, E_y^i(y') \sin k(y-y') \qquad (16a)$$

$$\int_{-l_1}^{l_1'} dy'\, I_1(y')\, \Pi(x,y') + \int_{-l_2}^{l_2} dx'\, I_2(x')\, \Pi(x,x')$$

$$= C_2 \cos kx + D_1 \sin kx - j \frac{4\pi}{\zeta} \int_0^x dx'\, E_x^i(x') \sin k(x-x') \qquad (16b)$$

and

$$\Pi(y,y') = \frac{\exp\left[-jk\sqrt{(y-y')^2 + a_1^2}\right]}{\sqrt{(y-y')^2 + a_1^2}} \qquad (17a)$$

$$\Pi(x,x') = \frac{\exp\left[-jk\sqrt{(x-x')^2 + a_2^2}\right]}{\sqrt{(x-x')^2 + a_2^2}} \qquad (17b)$$

$$\Pi(y,x') = -\int_0^y dy' \cos k(y-y') \frac{\partial G(y',x')}{\partial x'} \tag{17c}$$

$$\Pi(x,y') = -\int_0^x dx' \cos k(x-x') \frac{\partial G(x',y')}{\partial y'} \tag{17d}$$

where

$$G(y',x') = \frac{\exp\left[-jk\sqrt{x'^2 + y'^2 + a_1^2}\right]}{\sqrt{x'^2 + y'^2 + a_1^2}} \tag{18a}$$

$$G(x',y') = \frac{\exp\left[-jk\sqrt{x'^2 + y'^2 + a_2^2}\right]}{\sqrt{x'^2 + y'^2 + a_2^2}} \tag{18b}$$

and a_1 and a_2 are the radii of wires 1 and 2, respectively.

The remaining undefined terms in (16a) and (16b) are the integrals involving the incident electric field. For a single incoming plane wave directed toward the origin from the $z > 0$ space and in the (θ,ϕ) direction - these are the usual polar angles - there are two polarizations to be considered. These are the E and H polarizations; $\vec{E}$ in the x,y plane and $\vec{H}$ in the x,y plane, respectively. Figures 2 and 3 indicate the choice of phase angles for the two polarization states.

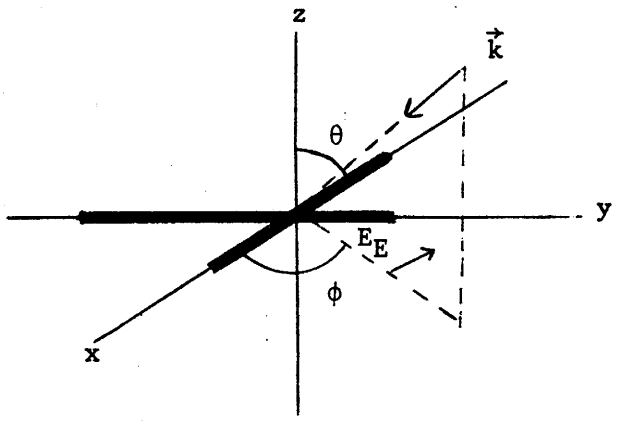

E Polarization

Figure 2

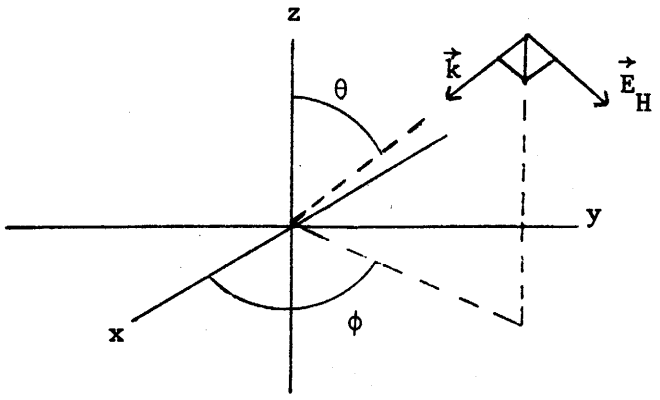

H Polarization

Figure 3

For E polarization

$$E_x^i(x') = E \cos(\phi + \pi/2) \exp\left[j\, k \sin\theta \cos\phi\, x'\right] \tag{19a}$$

$$E_y^i(y') = E \sin(\phi + \pi/2) \exp\left[j\, k \sin\theta \sin\phi\, y'\right] \tag{19b}$$

and for H polarization

$$E_x^i(x') = E \sin(\theta + \pi/2) \cos\phi \exp\left[j\, k \sin\theta \cos\phi\, x'\right] \tag{20a}$$

$$E_y^i(y') = E \sin(\theta + \pi/2) \sin\phi \exp\left[j\, k \sin\theta \sin\phi\, y'\right] \tag{20b}$$

This completes the definition of all terms in (16a) and (16b).

4. Numerical Results

In the actual analysis of the behavior of structures, the incoming plane wave of interest is considered to be composed of a symmetric portion and an antisymmetric portion whose sum reproduces the single incoming wave. The analysis is thus presented in terms of four cases: E-polarization, symmetric and antisymmetric; H-polarization, symmetric and antisymmetric (see Figures 4 and 5).

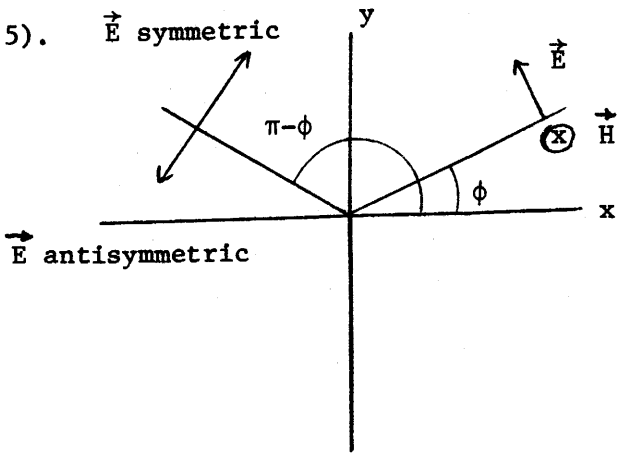

Figure 4

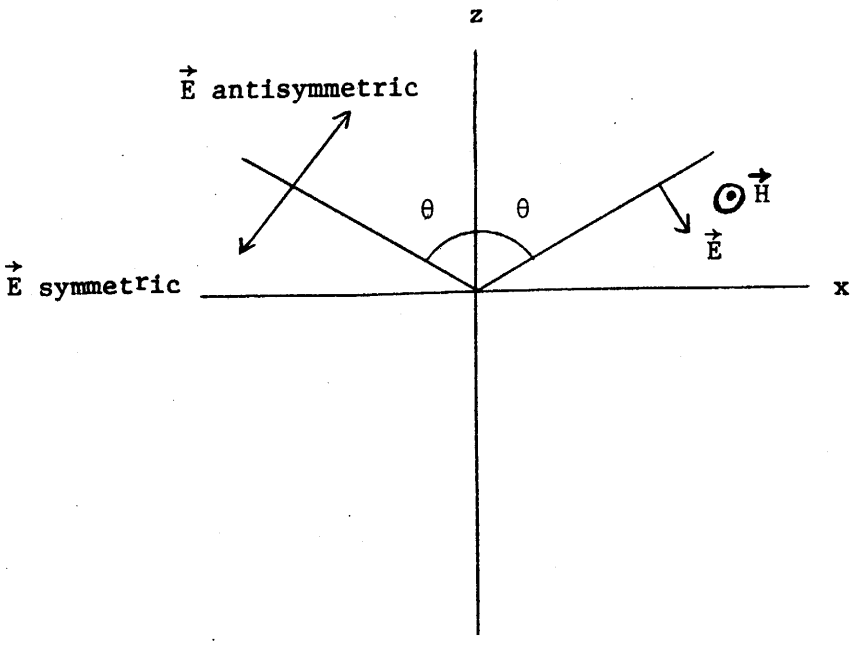

Figure 5

The treatment of a single incoming plane wave, amplitude E, at arbitrary angles of incidence (θ,ϕ) and arbitrary polarization proceeds in the following way. First, the E vector of the incoming wave is resolved into a component in the x,y plane (E-pol.) and a component perpendicular to $\vec{k}$ and the just defined E-polarization part. This now defines an E-polarization incoming wave, amplitude E_E, and an H-polarization incoming wave, amplitude E_H. Each of these waves is now resolved into symmetric and antisymmetric parts, each having magnitude $E_E/2$ for E-polarization and $E_H/2$ for H-polarization. Numerical results are presented in the form of currents and linear charge densities normalized by $2l_2$ and E_o where E_o is the amplitude of a single incoming wave and would be equal to $E_E/2$ or $E_H/2$ as the case may be. Thus for E-polarization the exciting field along wire 2 due to two incident waves (one at θ,ϕ; the other at $\theta,\pi-\phi$) and each having amplitude E_o becomes

$$E_x^i(x') = E_o \cos(\phi + \pi/2) \exp\left[j\, kx' \sin\theta \cos\phi\right]$$

$$+ E_o \cos\Delta \exp\left[j\, kx' \sin\theta \cos(\pi - \phi)\right]$$

and the symmetric and antisymmetric fields will be given by setting $\Delta = \pi/2 - \phi$ and $\Delta = 3\pi/2 - \phi$ in that order. The remaining field expressions (E-pol. on wire 1 and H-pol. on both wires) can be derived in a similar manner.

In the next section a specific numerical example is discussed that exhibits the manner in which the graphs can be used.

The numerical analysis is based on assuming the currents to be piecewise constant within a given zone of the structure. There results from this assumption a series of linear equations. The matrix form of the equations is

$$\Pi F = \Gamma$$

where F is a column matrix whose elements are the current magnitudes in the various zones and the C_n's and D_n's. Most of the elements of the (square) Π matrix are derived from the integral expressions of the left side of (16a) and (16b) and Γ is a column matrix determined by the integrals in (16a) and (16b) containing the incident field expressions.

5. Graphical Presentation

The reference case on which a great deal of information is plotted is

$$l_1'/l_1 = 0.5,\ 2l_2/(l_1+l_1') = 1.0,\ 2l_2/a = 20.0.$$

This case is run for values of kl_2 from 0.1 to 5.0 and for normal incidence. For any problem with normal incidence, E-polarization refers to excitation of wire 1 by the incoming wave while H-polarization refers to excitation of wire 2 by the incoming wave. Since wire 2 is always crossed at its mid-point by wire 1, for H-polarization there will be current only on wire 2. As further study shows in the case $l_1'/l_1 = 1.0$, there is complete uncoupling of the two elements for these polarizations.

All curves are for incoming plane waves of amplitude E_o v/m. For normal incidence there are two waves as in every angle case, and the rules of section 4 must be followed to determine the effects of a single plane wave noting E antisymmetric and H symmetric currents are always zero for normal incidence. Figures (7-16) represent the currents on different parts of the structure as functions of kl_2 for the reference case. To exhibit explicitly the manner in which these curves should be used, suppose one wishes to determine the junction current on wire 2 for $kl_2 = 1.15$ and a single incoming plane wave of amplitude 1 v/m and E-polarization. This incoming plane wave will be formed by an E symmetric part, amplitude 0.5 v/m, and an E antisymmetric part, amplitude 0.5 v/m. From Figure 7, the magnitude of $I/(2l_2E_o)$ is 0.0117 amperes/volt and the phase is zero. Thus, for a structure of unit length ($2l_2$ = 1m) and E_o = 0.5 v/m, the complex current due to the symmetric wave is $(5.85 + j\ 0) \times 10^{-3}$ amps and the complex current due to the antisymmetric wave is zero. Therefore the complex junction current on wire 2 for a plane wave, E-polarization, E = 1 v/m, is (5.85 + j 0) ma. Figure 8 represents the magnitude and phase of the complex current on wire 2 at a position one-third of the way from the junction to

the end of wire 2. Other locations are similarly defined. Figures (17-22) represent the linear charge densities, λ (coulombs/meter), on various parts of the structure as a function of kl_2 for the reference case.

Figures (23-26) fall into a category different from others in this report. These curves are time histories of junction currents on the structure as functions of $ct/2l_2$. These are the result of a Fourier inversion of the frequency spectrum assuming an incoming pulse of the form

$$E(t) = E_o\, U(t)\, e^{-\alpha t} \qquad \alpha = 0.1/\text{sec}$$

where U(t) is the unit step function defined by

$$U(t) = 0 \qquad t \leq 0$$

$$U(t) = 1 \qquad t > 0$$

The pulse of interest is the step function but for mathematical convenience a slowly decreasing exponential is included in this definition. In the case of these time histories, the value of $2l_2$ is defined to be unit magnitude. Thus Figures (7-26) refer to the reference case.

Figures (27-28) exhibit the resonant length variations as the crossing point location varies from an approximate T-structure ($l_1'/l_1 = 0.1$) to crossing at the geometric center ($l_1'/l_1 = 1.0$). In these figures the resonant length is defined as the value of kl_2 at which the largest magnitude of the junction currents occurs. Figures (29-30) show the manner in which the magnitudes of the junction currents evaluated at their resonant frequencies vary as l_1'/l_1 varies. For example, on Figure 29 the value for $I_{RES}/2l_2\, E_o$ at $l_1'/l_1 = 0.5$ is determined from the magnitude curve on Figure 7. Figures

(31-32) illustrate the dependence of the maximum junction currents in time [$=I_{MAX}(t)$] on $1_1'/1_1$, as determined from figures such as Figure 23.

Figures (33-34) demonstrate the behavior of the resonant linear charge densities (λ_{RES}) - where $\lambda_{RES}/21_2E_o$ is determined by observing the peak values on curves such as Figure 18 - as functions of $1_1'/1_1$. Figures (35-36) signify those values of kl_2 - called resonant length (λ) - at which λ_{RES} occurs versus $1_1'/1_1$. Note that resonant length always refers to values of kl_2 at which junction currents are maximum, while resonant length (λ) refers to values of kl_2 for which linear charge densities are maximum. Thus Figures (37-40) present variations of resonant length and resonant length (λ) as $21_2/(1_1'+1_1)$ varies from 0.5 up to 1.2. Figures (41-43) show I_{RES} and λ_{RES} variations as functions of $21_2/(1_1'+1_1)$, while Figures (44-48) display variations of $I_{MAX}(t)$ and $\lambda_{MAX}(t)$ - the maximum linear charge density in time - as functions of the same variable.

Figures (49-56) display currents at various points on the structure for the different polarizations at non-normal incidence. Figures (57-59) clearly exhibit the effects of the thin wire approximations as the radius of the wires changes. Figures (60-62) display the behavior of the system when wires having different radii are considered, a_i referring to the radius of wire i. Notice there are no curves for H-polarization as a_1/a_2 varies - this is because the current remained constant on wire 2 since a_2 was held constant and a_1 accounted for the varying ratio, a_1/a_2.

While an exhaustive study of zone size has not been run on the crossed-wire problem, certain data are of interest. In Figure 29, I_{RES} for H-polarization provides useful information on this question. I_{RES}(H-pol.) should be independent of $1_1'/1_1$ due to geometric considerations. Due to the numerical techniques used in solving this problem, the number of zones on wire 2

varies (in this figure) from 38 for $1_1'/1_1 = 0.8$ to 62 for $1_1'/1_1 = 0.5, 1.0$. Notice that $I_{RES}/21_2E_o$ has the value $(22.7 \pm .2) \times 10^{-3}$ amperes/volt for all values of $1_1'/1_1$. It is also of interest to note the λ_{RES}(H-pol.) variations on Figure 33. Again this should be a straight line but due to the manner in which the charge density is determined and zoning variations, one must conclude that the charge densities are not as good as the currents calculated. Figure 34 also points out the sensitivity of charge density calculations - on wire 1 ($y > 0$) calculations, the number of zones varies from 31 for $1_1'/1_1 = 1.0$ to 5 for $1_1'/1_1 = 0.1$. It must be observed that the size of the zones does not vary nearly this much as a function of $1_1'/1_1$ - the zone size goes only from 0.01667 to 0.02778.

In a separate but related investigation on a single linear antenna ($21_2/a = 20$), the number of zones on the structure was varied from 20 to 80 and currents induced on the structure by a normally incident plane were calculated. This study showed that over 80% of the length of the antenna the current values calculated for 40 and 80 zones were the same to within 7% toward the ends of the antenna and within 4% at the center of the antenna. It has been shown that the use of an axial current that is independent of the actual cross-sectional distribution of current provides accurate results as long as the point of interest is not within five (5) radii of the end of the structure [3]. In the crossed wire program the minimum number of zones on a given wire (1 or 2) was 38. However, the effects of intersecting wires and numbers of zones on each side of the intersection may well be more important than the total number of zones on the wire.

Literature Cited

1. Mei, K. K., ON THE INTEGRAL EQUATIONS OF THIN WIRE ANTENNAS, IEEE Trans. Ant. Prop., Vol. AP-13, No. 3, 1965, pp 374-378.
2. Taylor, C. D., ELECTROMAGNETIC SCATTERING FROM ARBITRARY CONFIGURATIONS OF WIRES, IEEE Trans. Ant. Prop., Vol. AP-17, No. 5, 1969, pp 662-663.
3. King, R. W. P., THE THEORY OF LINEAR ANTENNAS, Harvard University Press, Cambridge, Massachusetts (1956).

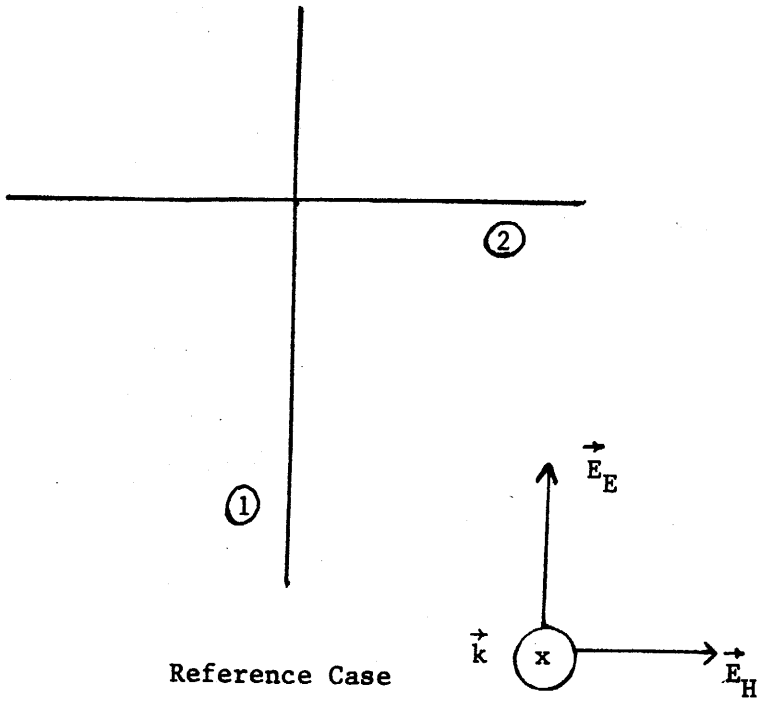

Reference Case

Figure 6

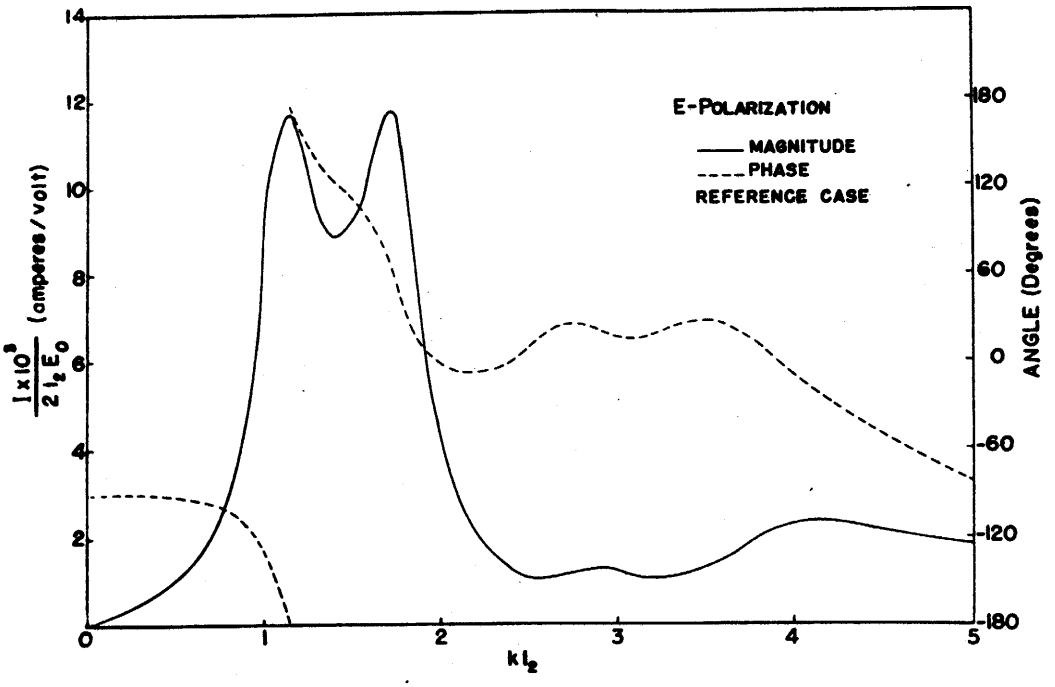

FIGURE 7. Junction current on wire 2 vs kl_2.

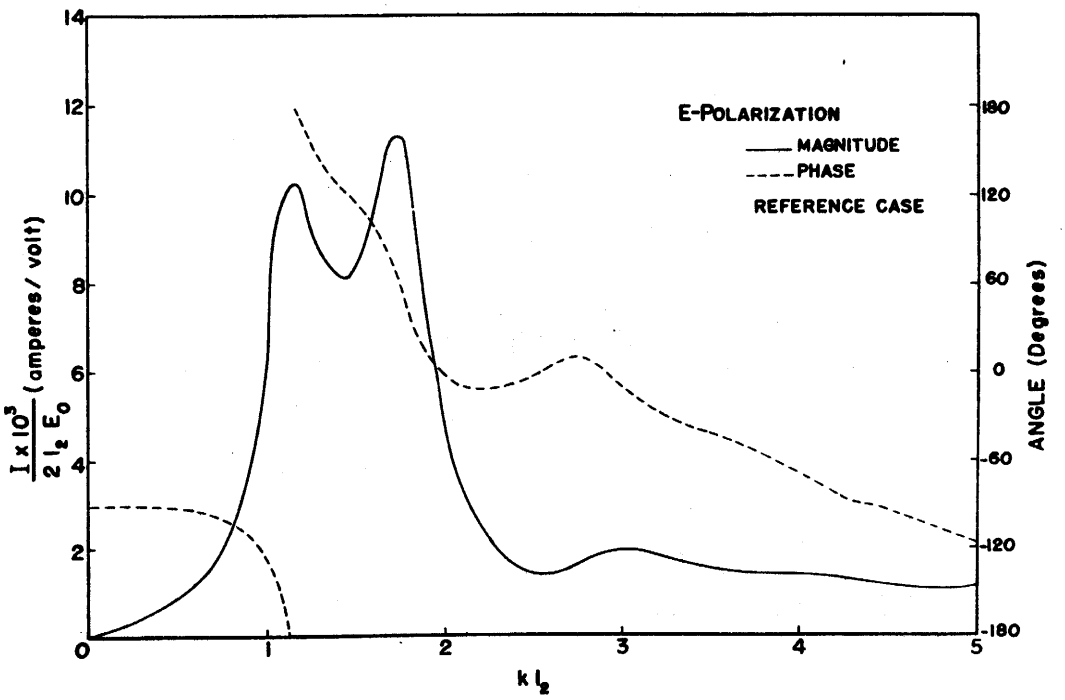

FIGURE 8. Current on wire 2 at 0.333 l_2 vs kl_2.

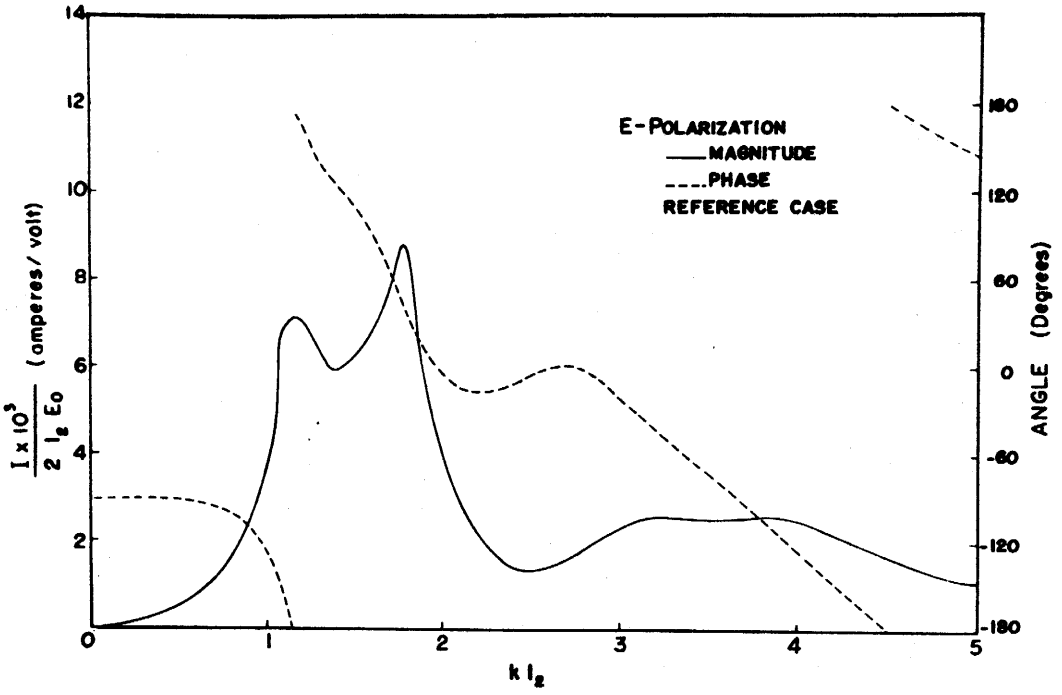

FIGURE 9. Current on wire 2 at 0.667 l_2 vs kl_2.

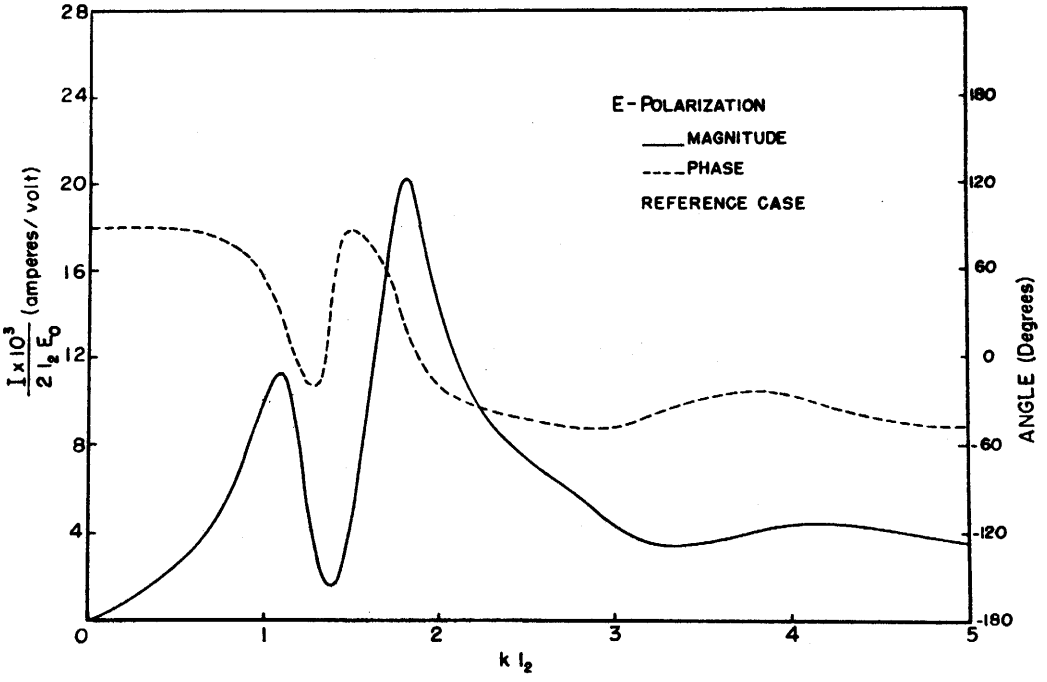

FIGURE 10. Junction current ($y=0^+$) on wire 1 vs kl_2.

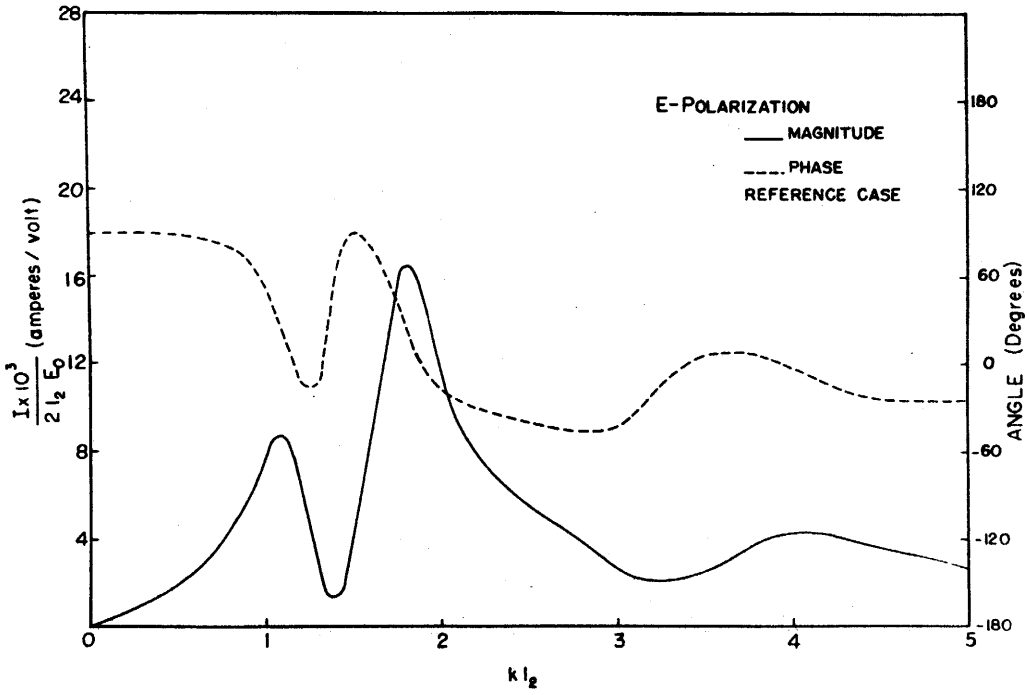

FIGURE 11. Current on wire 1 at 0.50 l_1' vs kl_2.

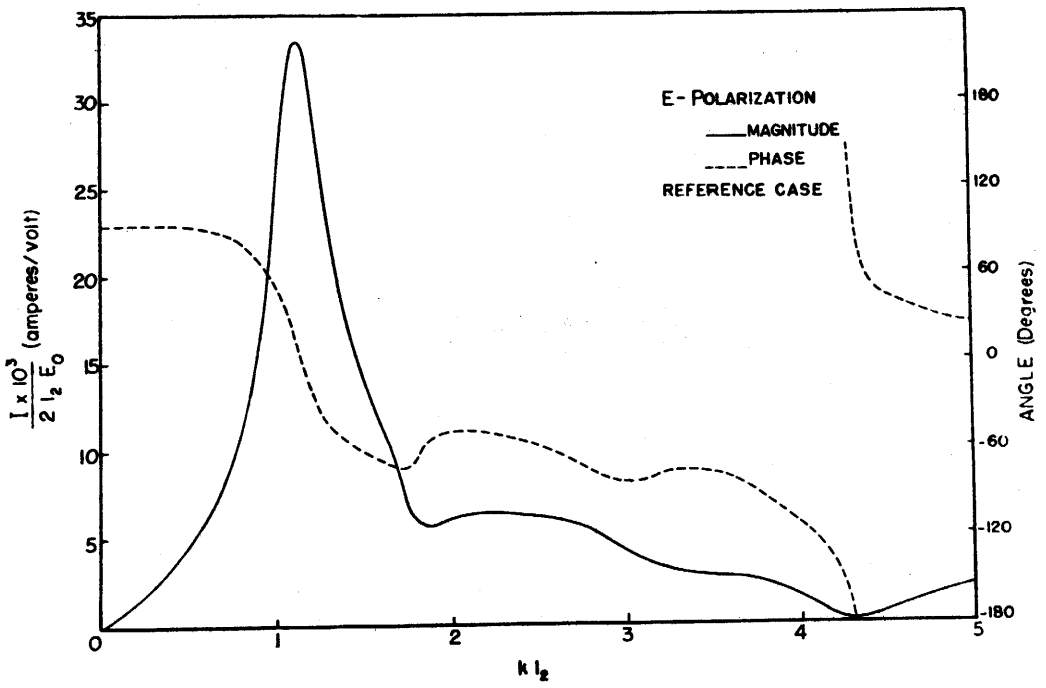

FIGURE 12. Junction current ($y=0^-$) on wire 1 vs kl_2.

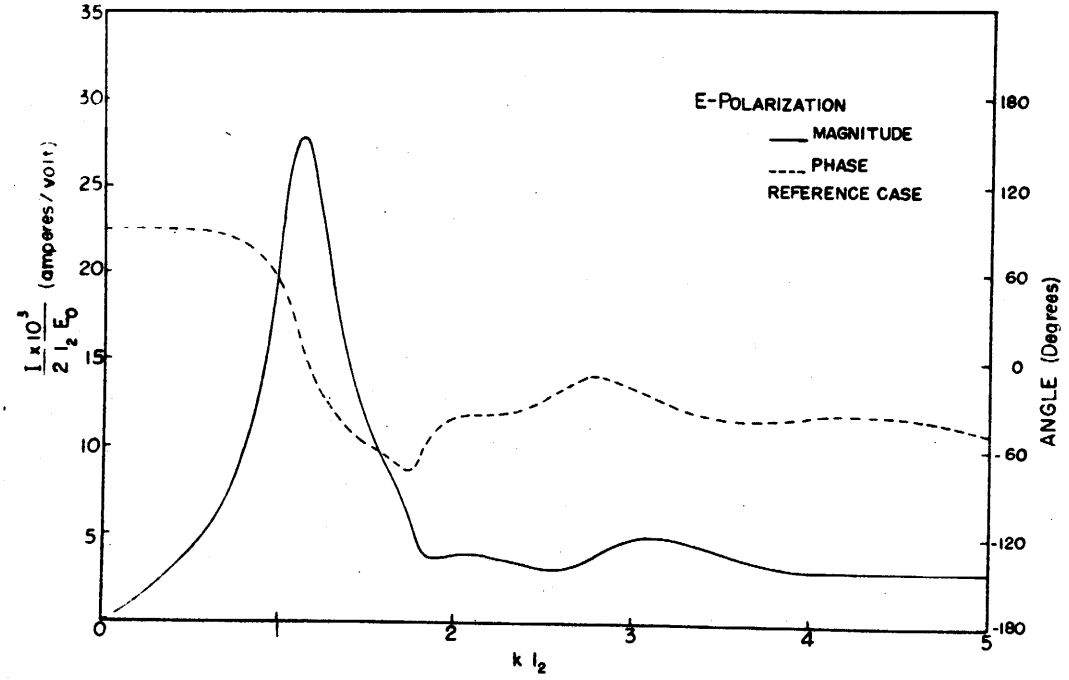

FIGURE 13. Current on wire 1 at 0.50 l_1 vs kl_2.

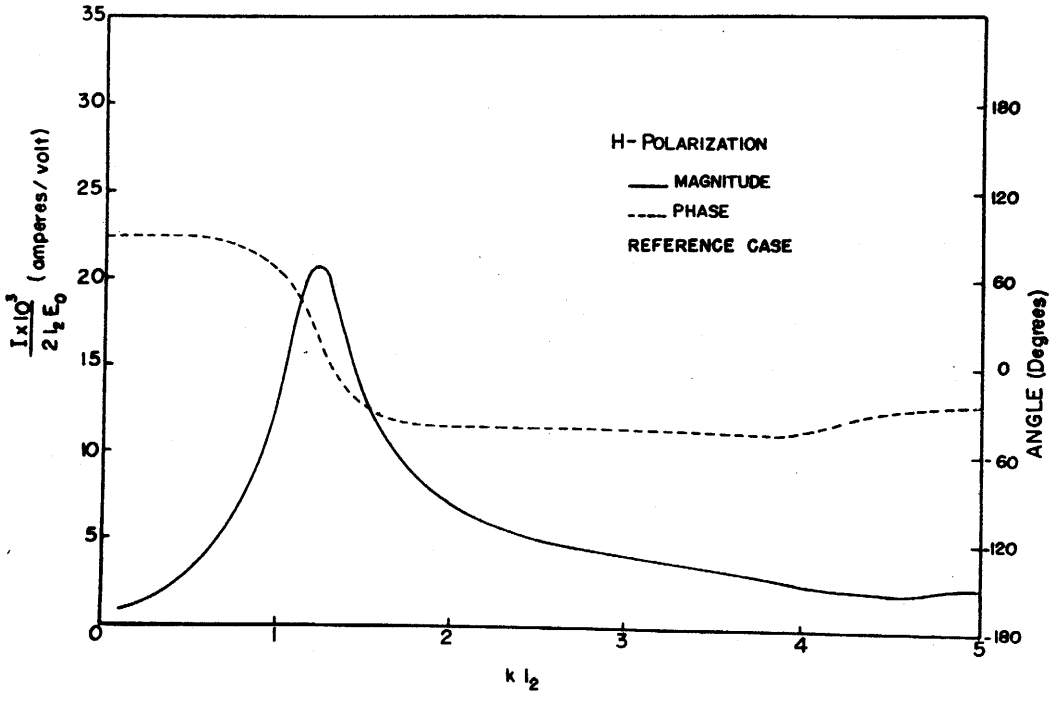

FIGURE 14. Junction current on wire 2 vs kl_2.

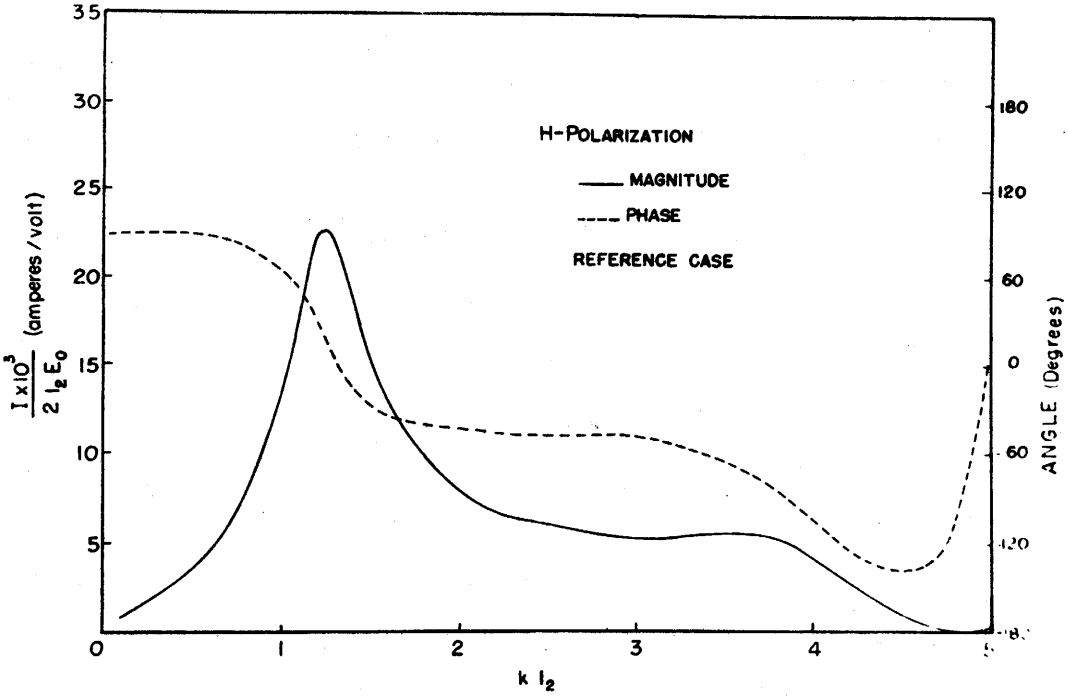

FIGURE 15. Current on wire 2 at 0.333 l_2 vs kl_2.

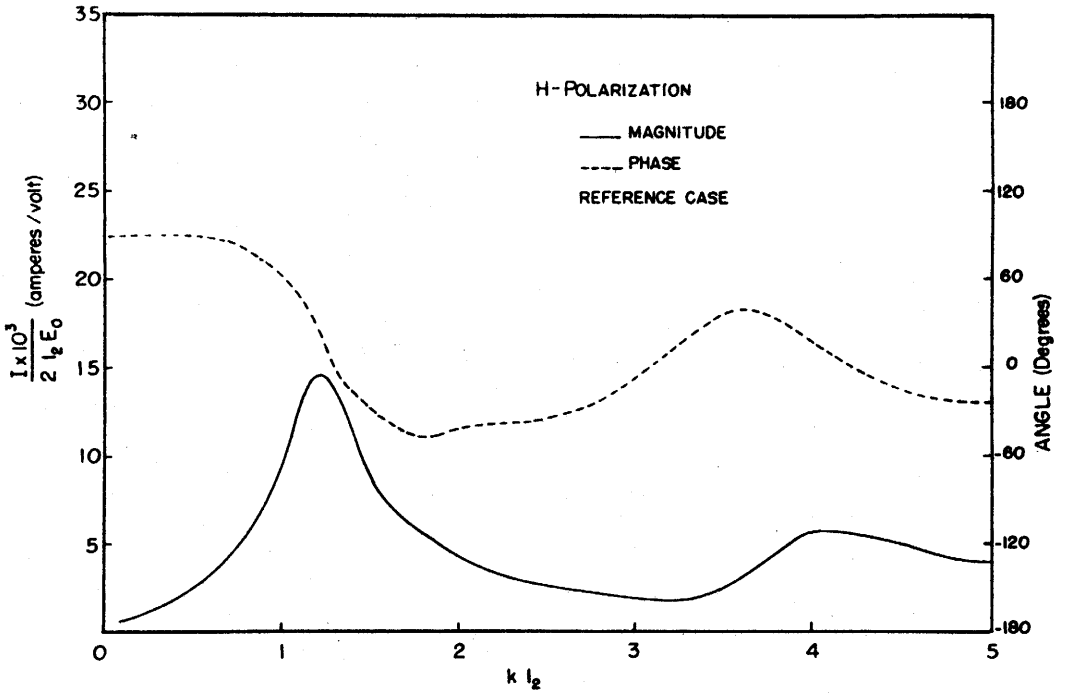

FIGURE 16. Current on wire 2 at 0.667 l_2 vs kl_2.

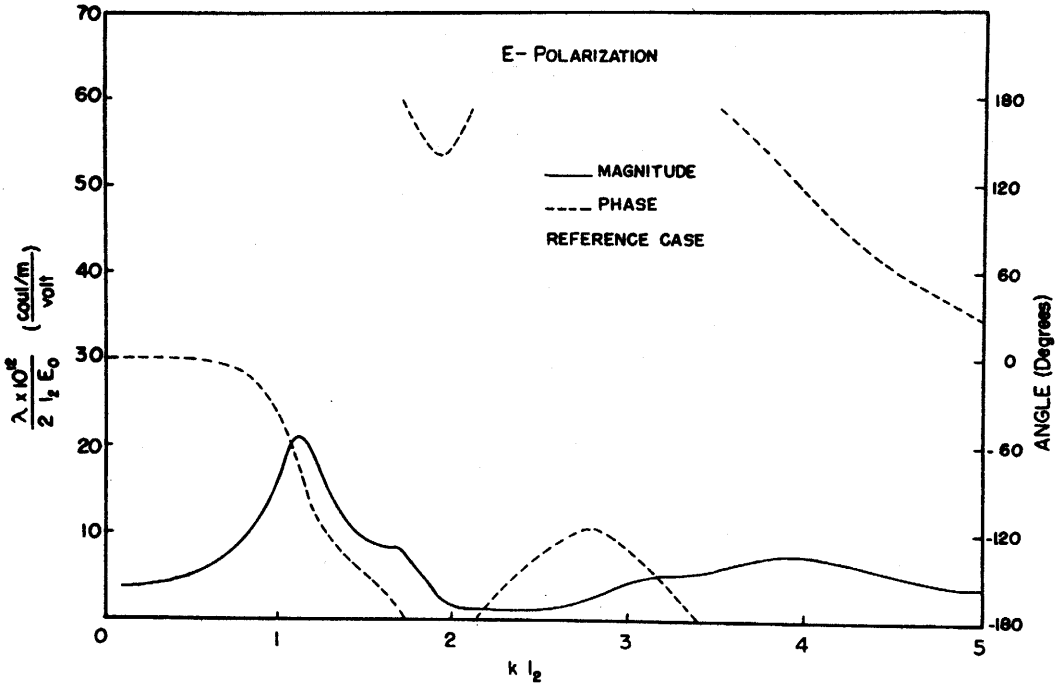

FIGURE 17. Linear charge density on wire 2 at 0.333 l_2 vs kl_2.

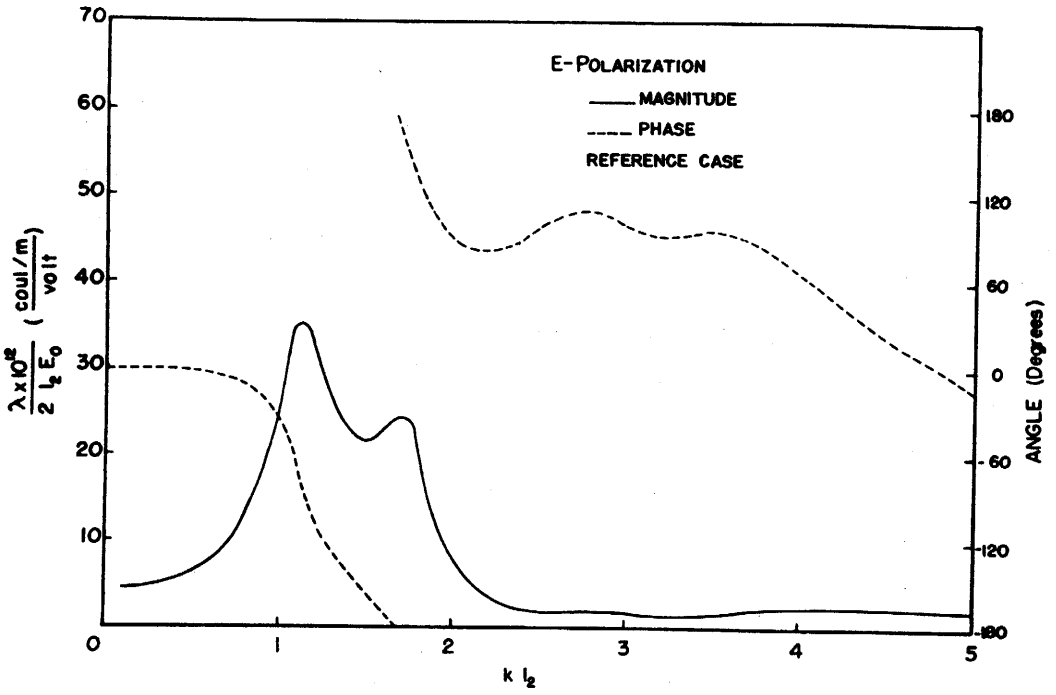

FIGURE 18. Linear charge density on wire 2 at 0.667 l_2 vs kl_2.

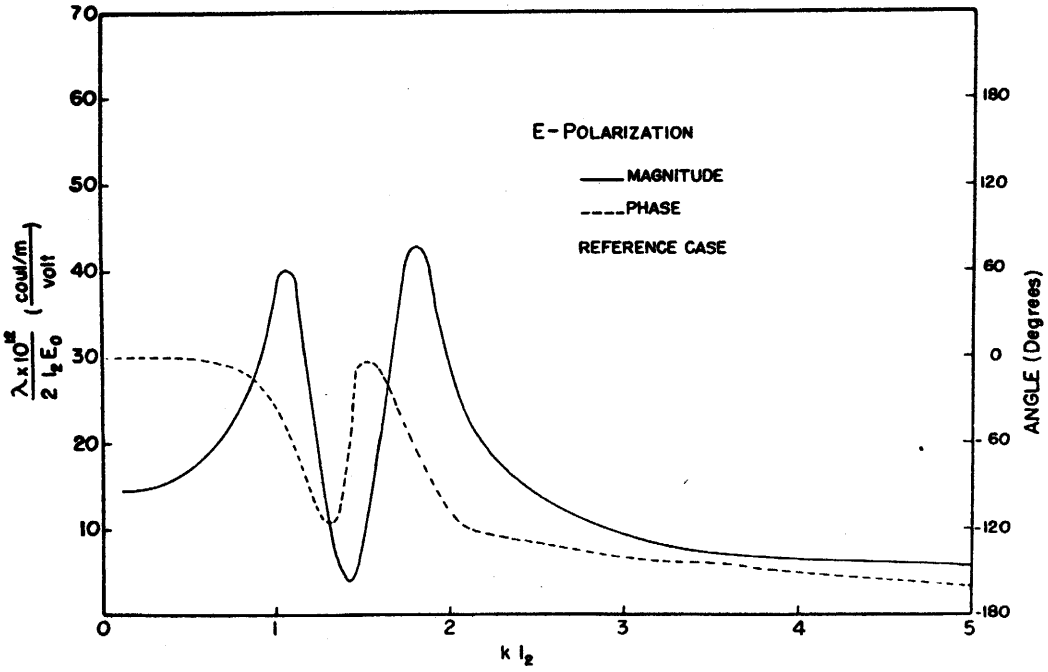

FIGURE 19. Linear charge density on wire 1 at 0.50 l_1' vs kl_2.

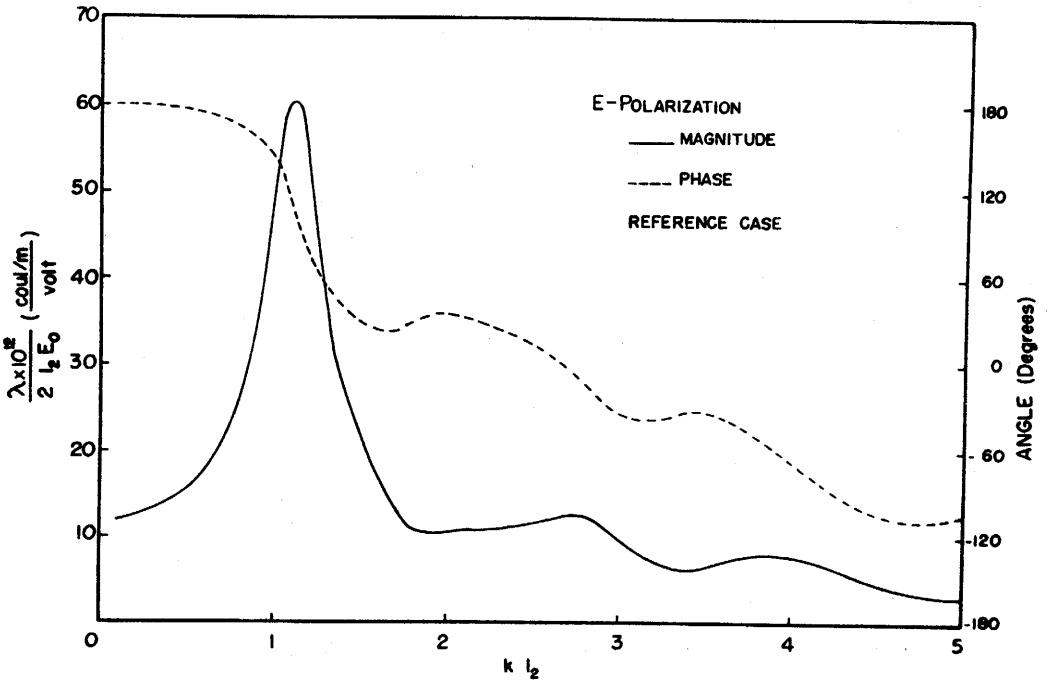

FIGURE 20. Linear charge density on wire 1 at 0.50 l_1 vs kl_2.

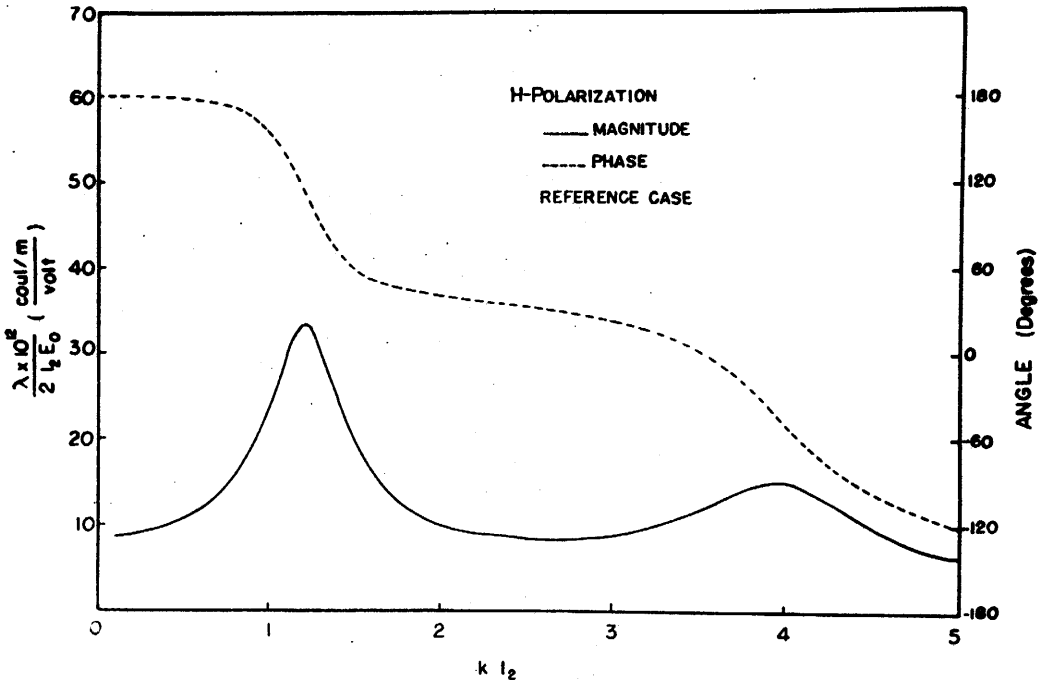

FIGURE 21. Linear charge density on wire 2 at 0.333 l_2 vs kl_2.

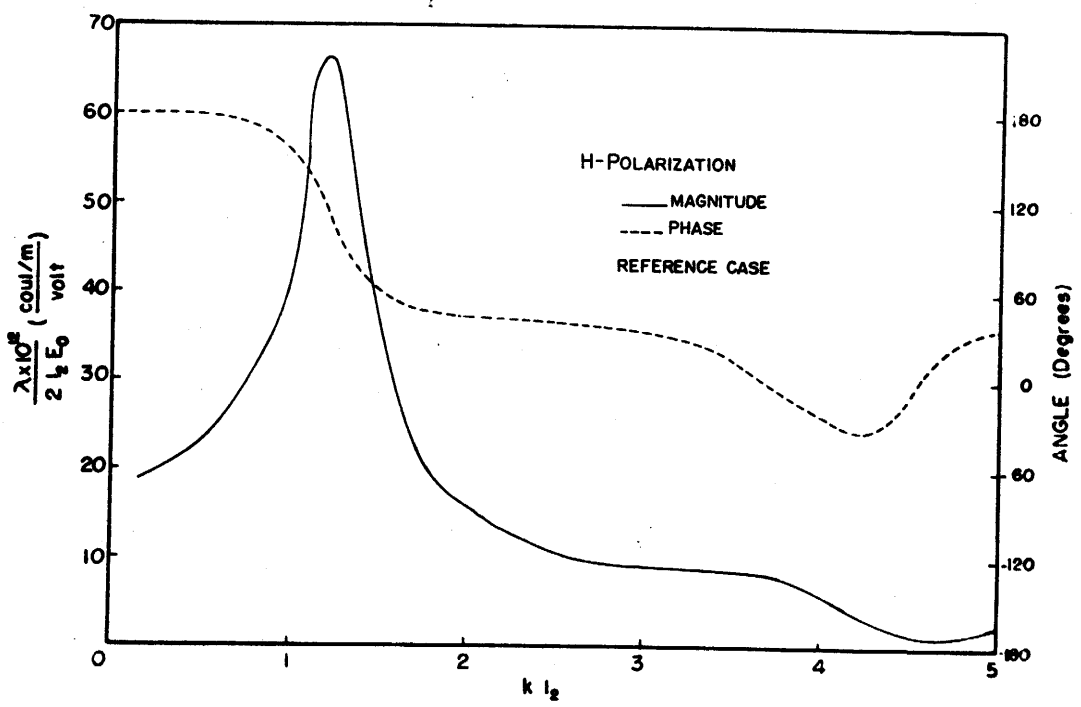

FIGURE 22. Linear charge density on wire 2 at 0.667 l_2 vs kl_2.

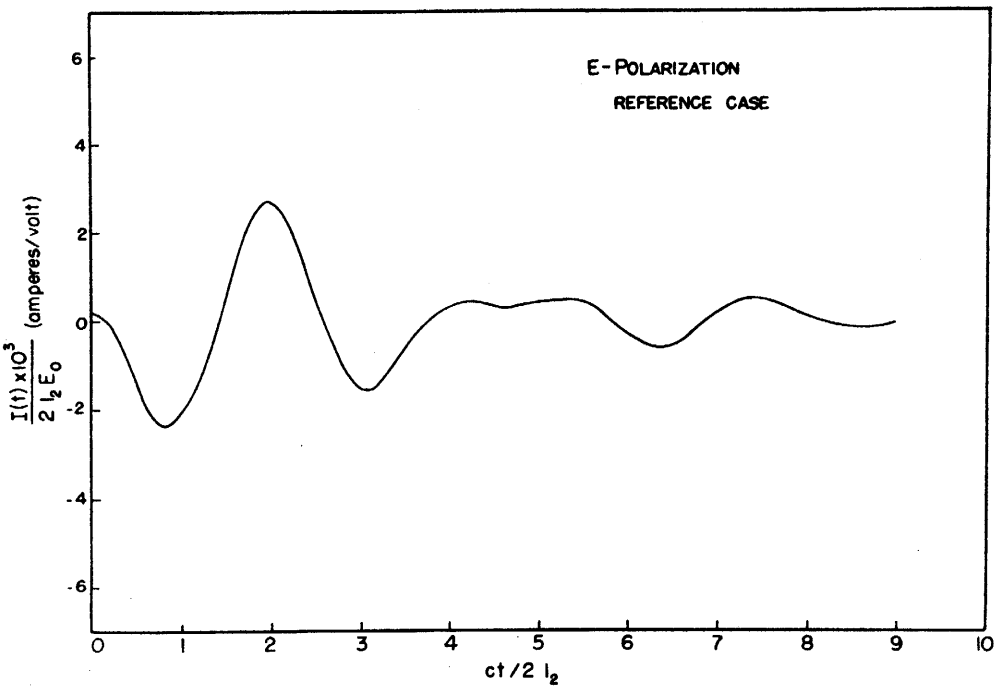

FIGURE 23. Junction current on wire 2 vs $ct/21_2$.

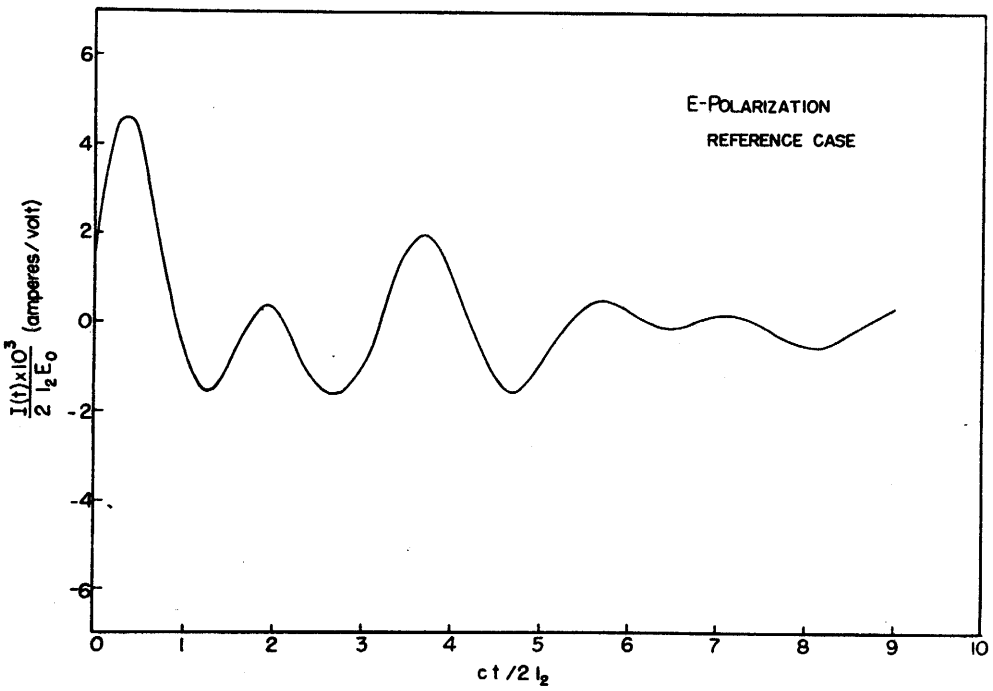

FIGURE 24. Junction current ($y=0^+$) on wire 1 vs $ct/21_2$.

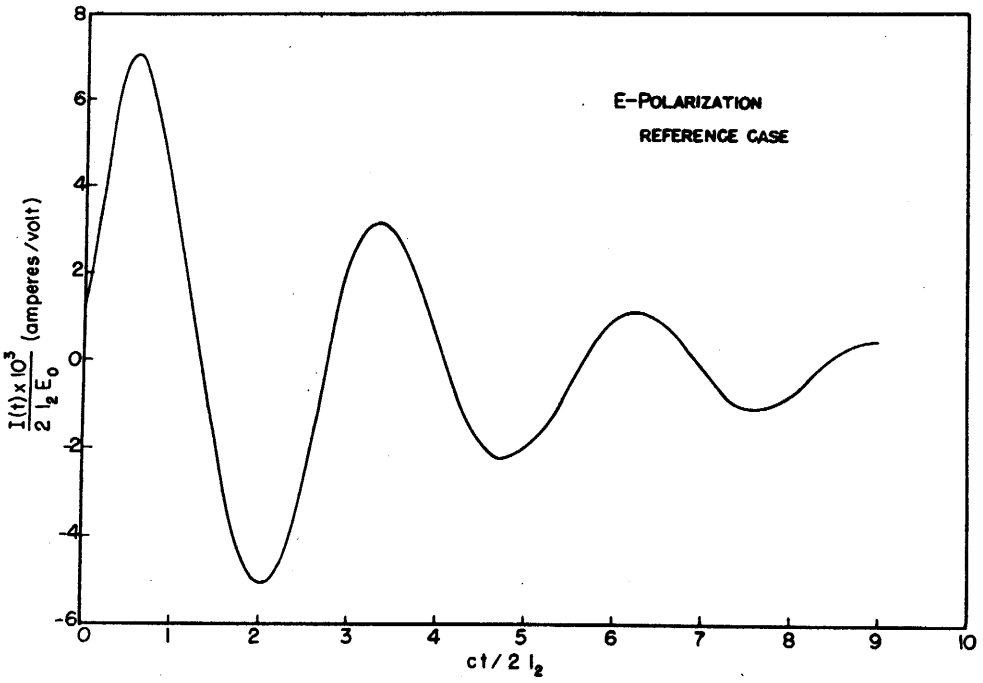

FIGURE 25. Junction current ($y=0^-$) on wire 1 vs $ct/21_2$.

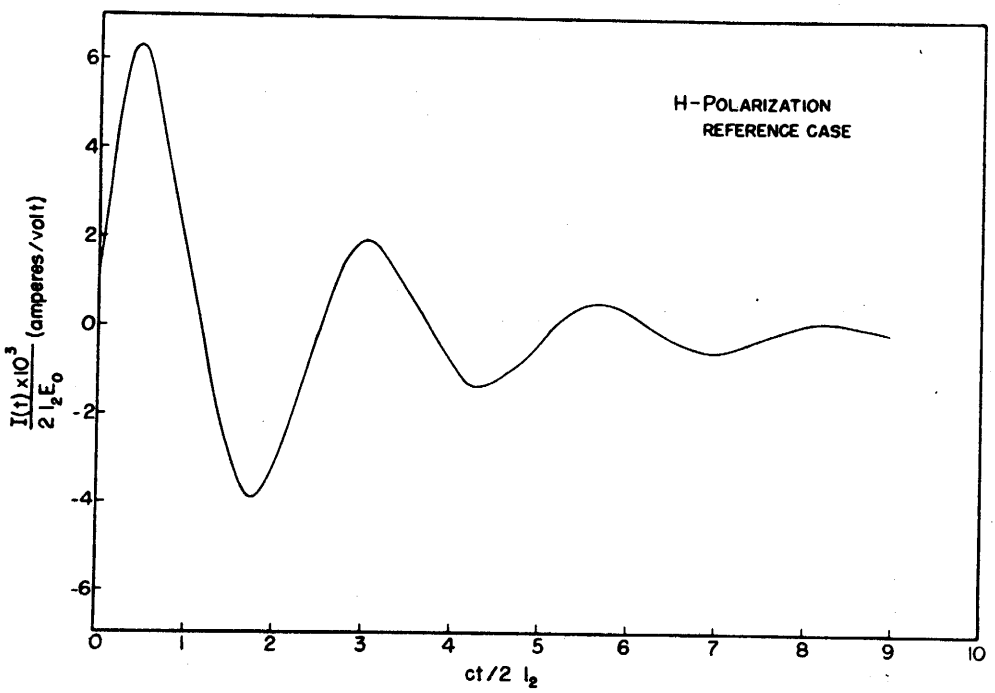

FIGURE 26. Junction current on wire 2 vs $ct/21_2$.

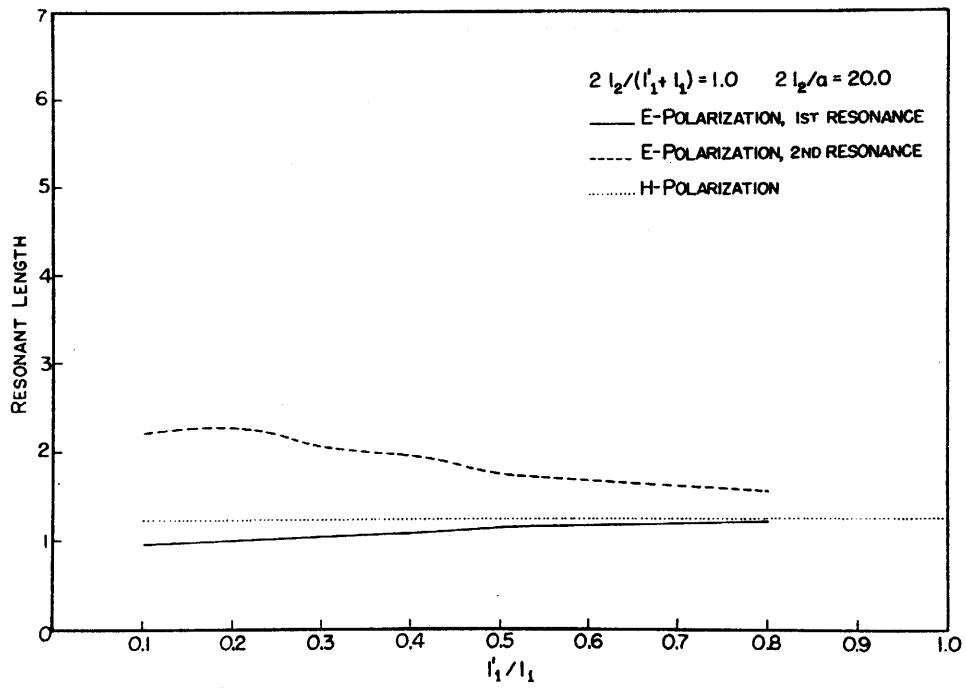

FIGURE 27. Resonant lengths of wire 2 for junction current vs l_1'/l_1.

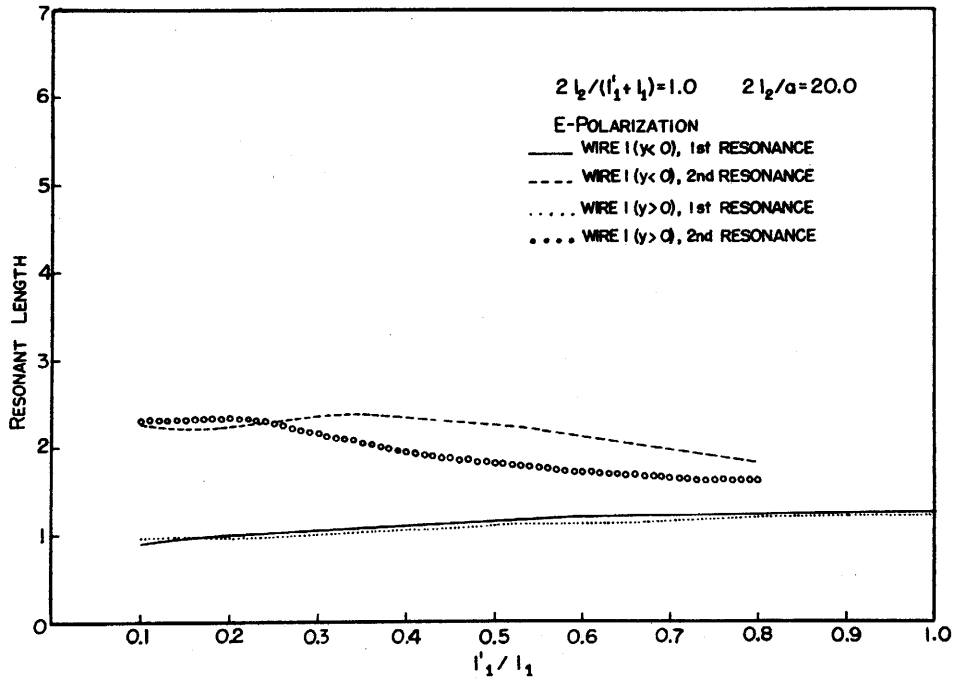

FIGURE 28. Resonant lengths of wire 1 for junction current vs l_1'/l_1.

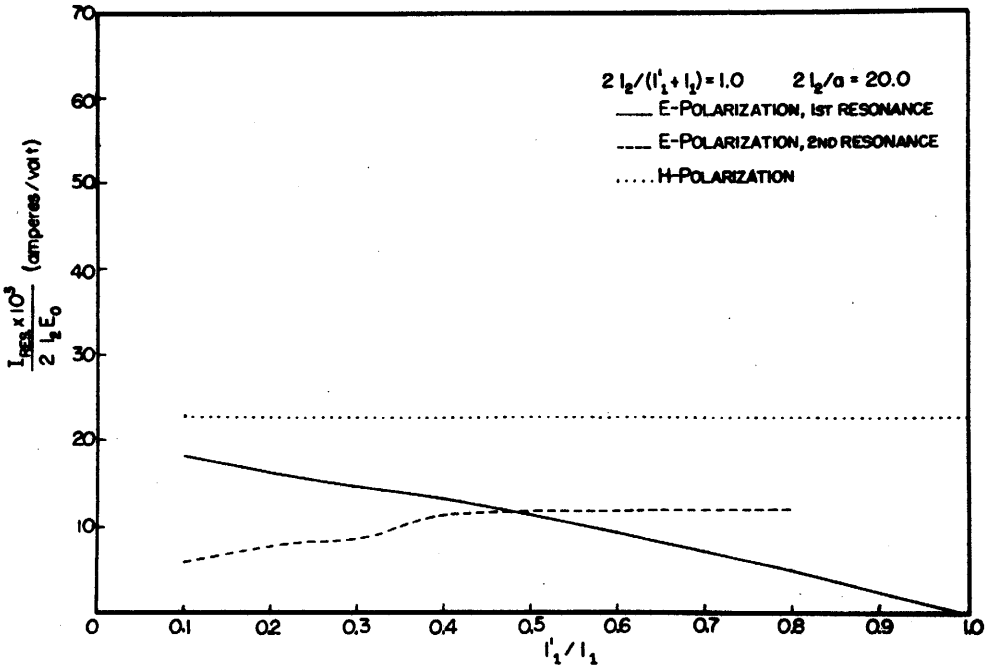

FIGURE 29. Resonant junction currents on wire 2 vs $1_1'/1_1$.

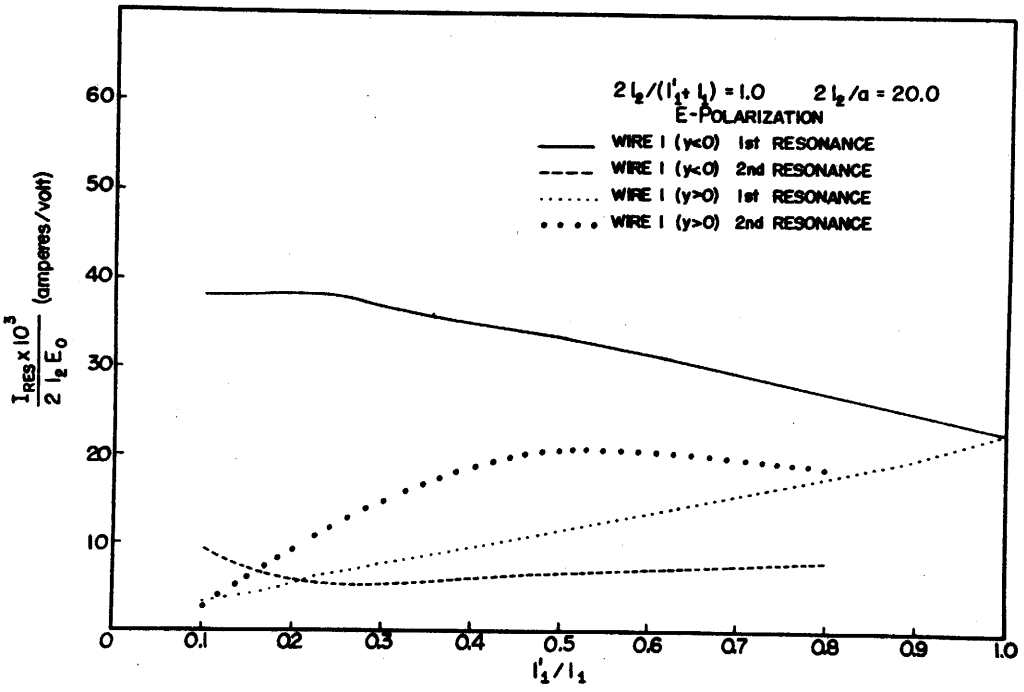

FIGURE 30. Resonant junction currents on wire 1 vs $1_1'/1_1$.

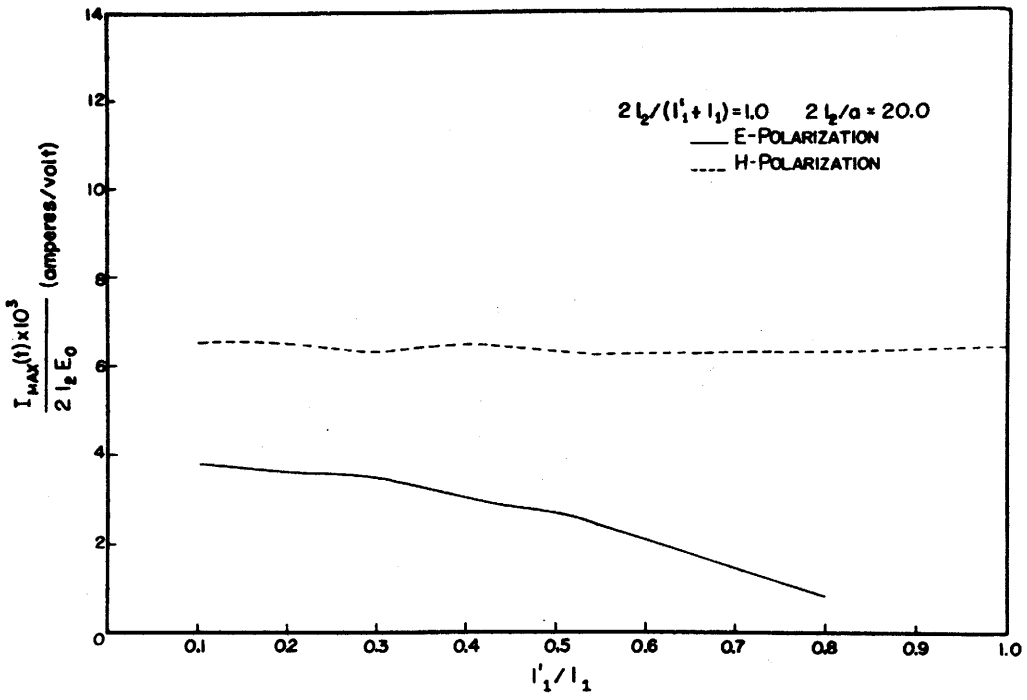

FIGURE 31. Maximum junction currents in time on wire 2 vs $1_1'/1_1$.

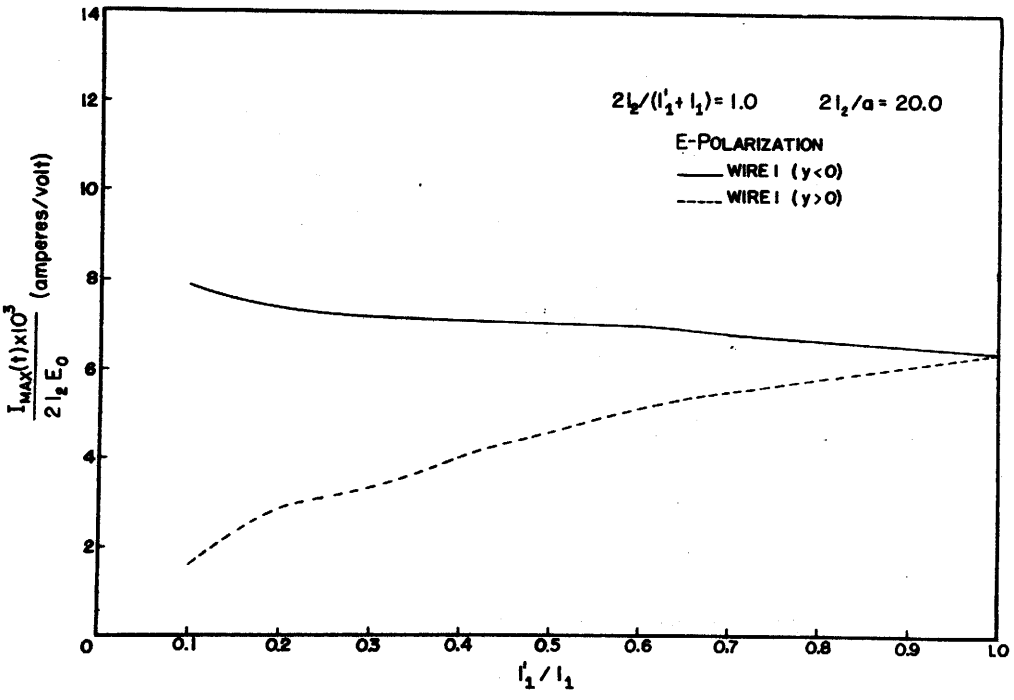

FIGURE 32. Maximum junction currents in time on wire 1 vs $1_1'/1_1$.

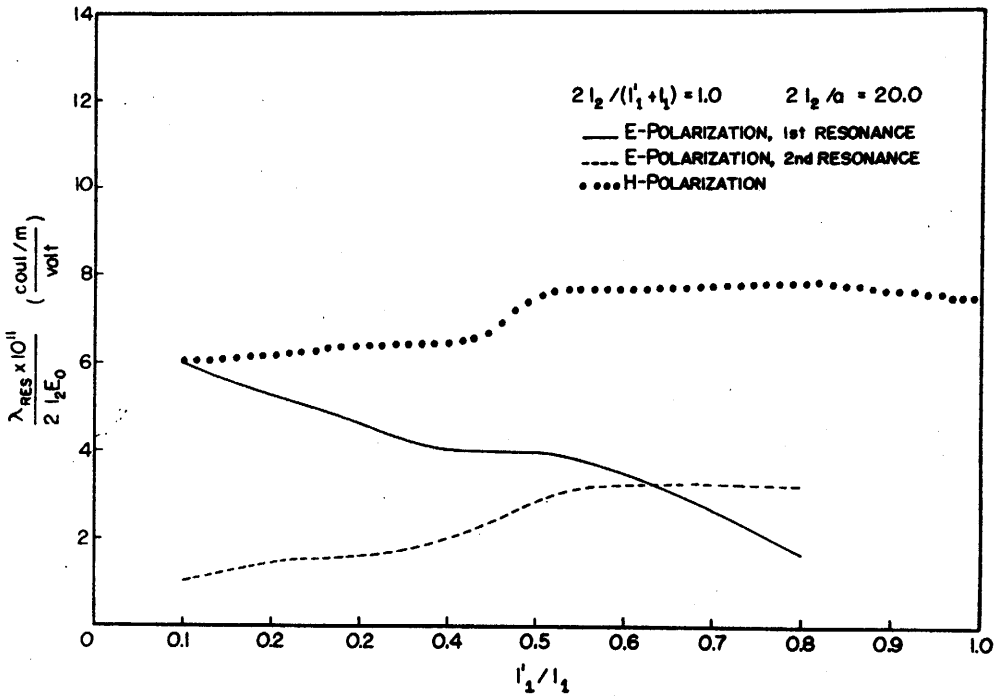

FIGURE 33. Resonant linear charge densities on wire 2 at ~0.7 l_2 vs l_1'/l_1.

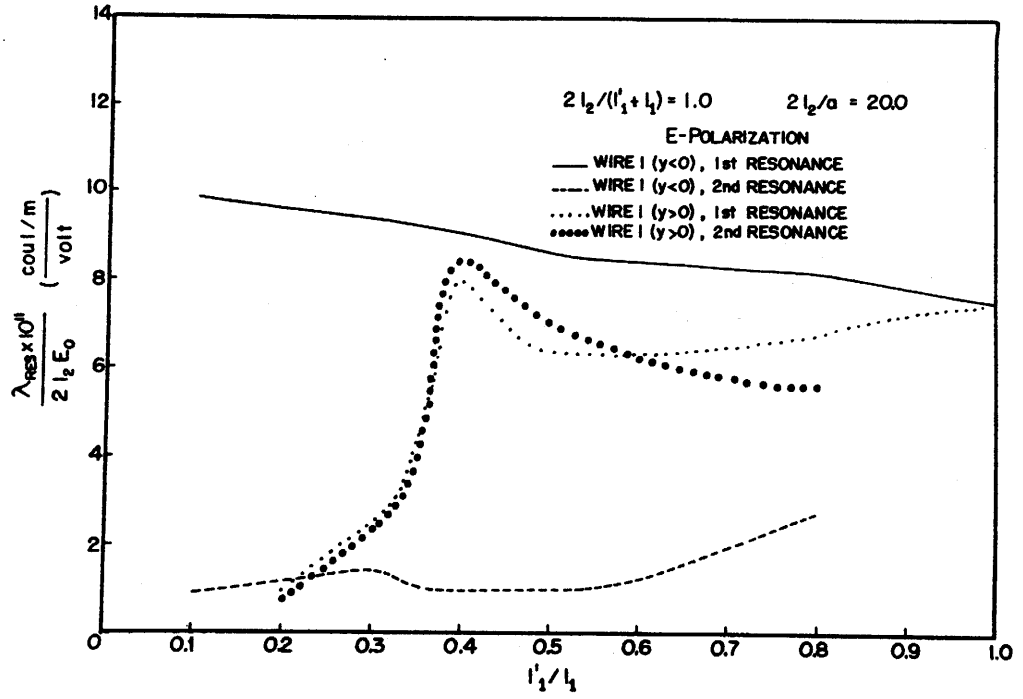

FIGURE 34. Resonant linear charge densities on wire 1 at ~0.7 l_1 and ~0.7 l_1' vs l_1'/l_1.

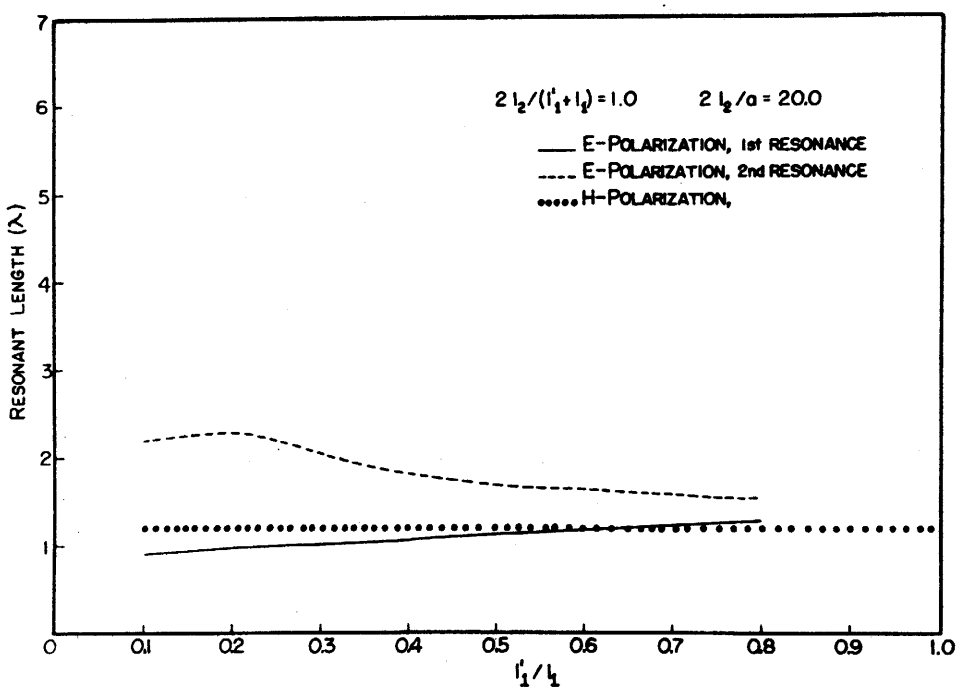

FIGURE 35. Resonant lengths (λ) of wire 2 for linear charge density at ~0.7 l_2 vs l_1'/l_1.

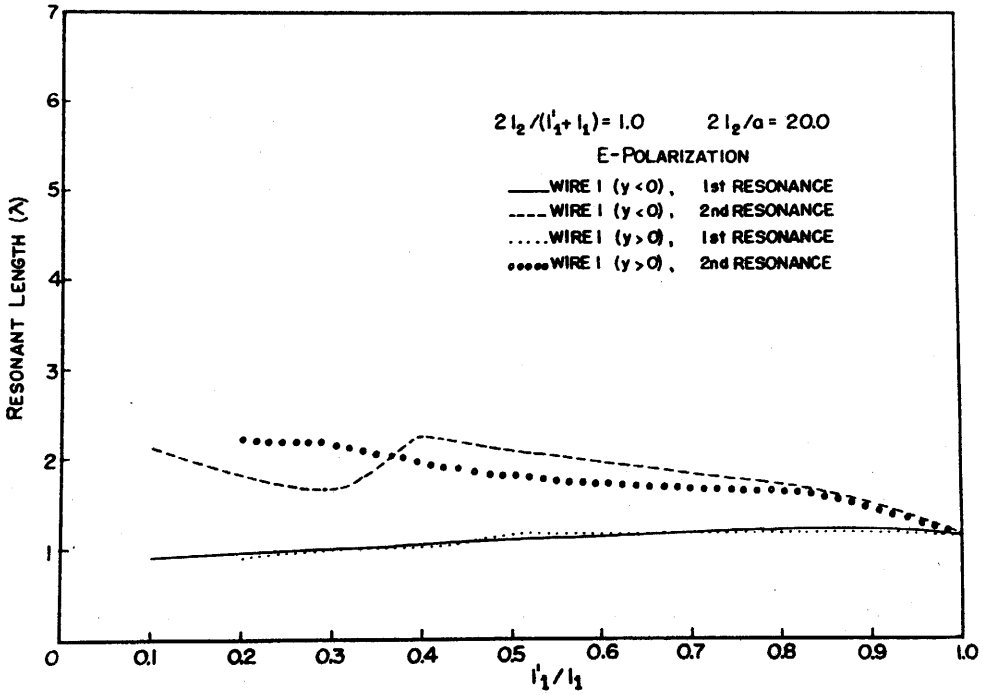

FIGURE 36. Resonant lengths (λ) of wire 1 for linear charge density at ~0.7 l_1 and ~0.7 l_1' vs l_1'/l_1.

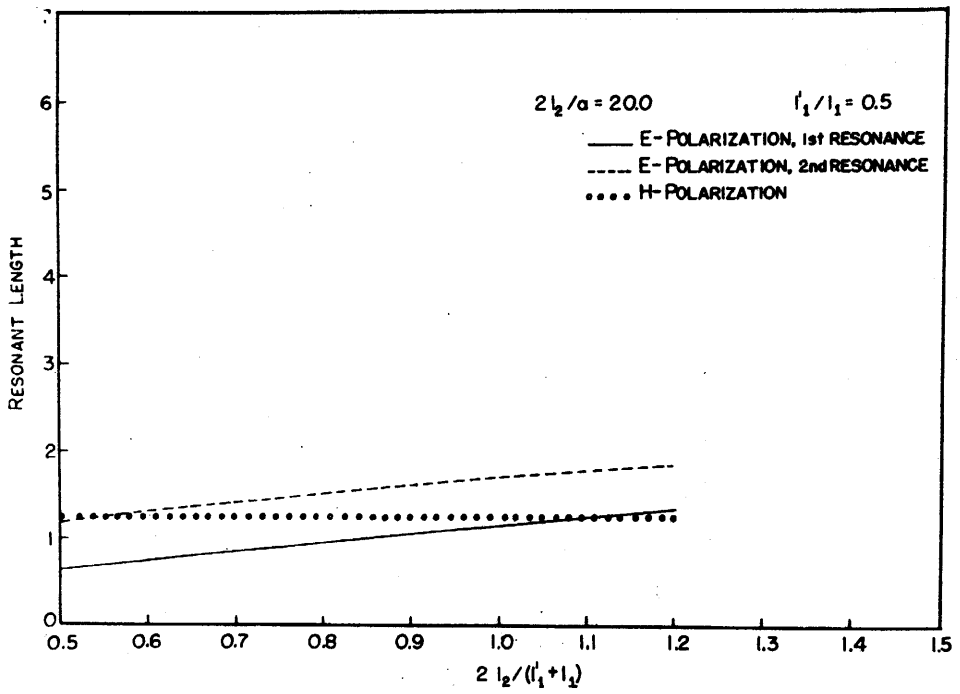

FIGURE 37. Resonant lengths of wire 2 for junction current vs $2l_2/(l'_1+l_1)$.

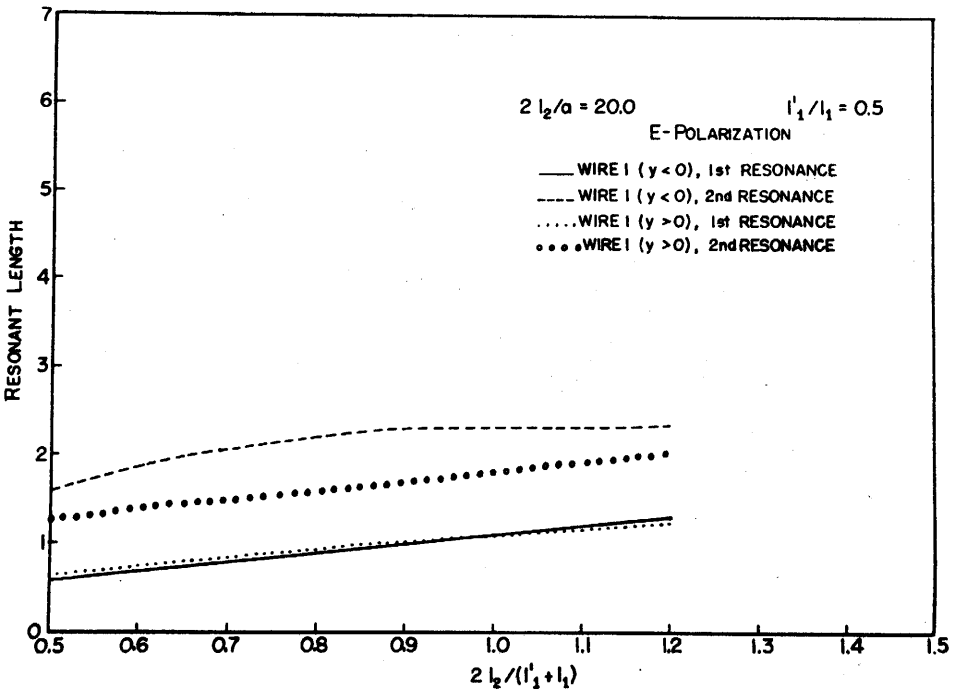

FIGURE 38. Resonant lengths of wire 1 for junction current vs $2l_2/(l'_1+l_1)$.

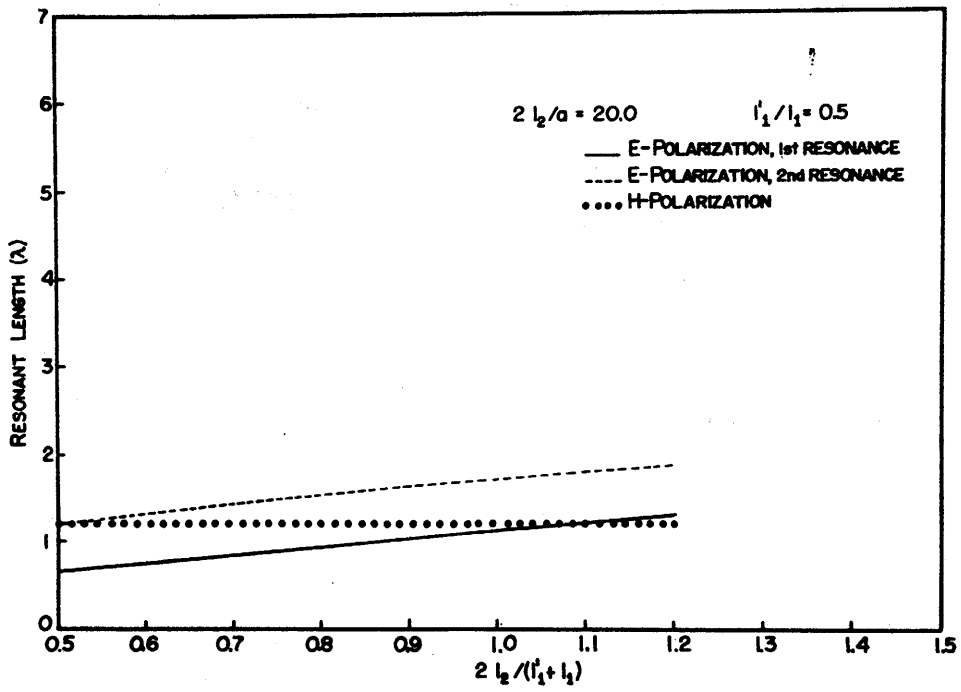

FIGURE 39. Resonant lengths (λ) of wire 2 for linear charge density at ~0.7 l_2 vs $2l_2/(l_1'+l_1)$.

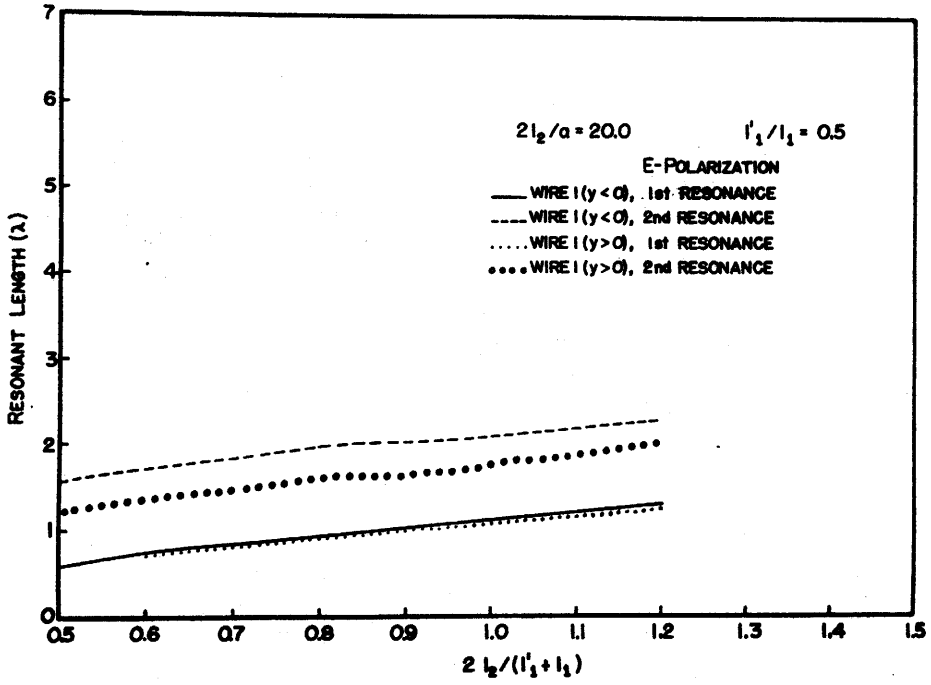

FIGURE 40. Resonant lengths (λ) of wire 1 for linear charge density at ~0.7 l_1 and ~0.7 l_1' vs $2l_2/(l_1'+l_1)$.

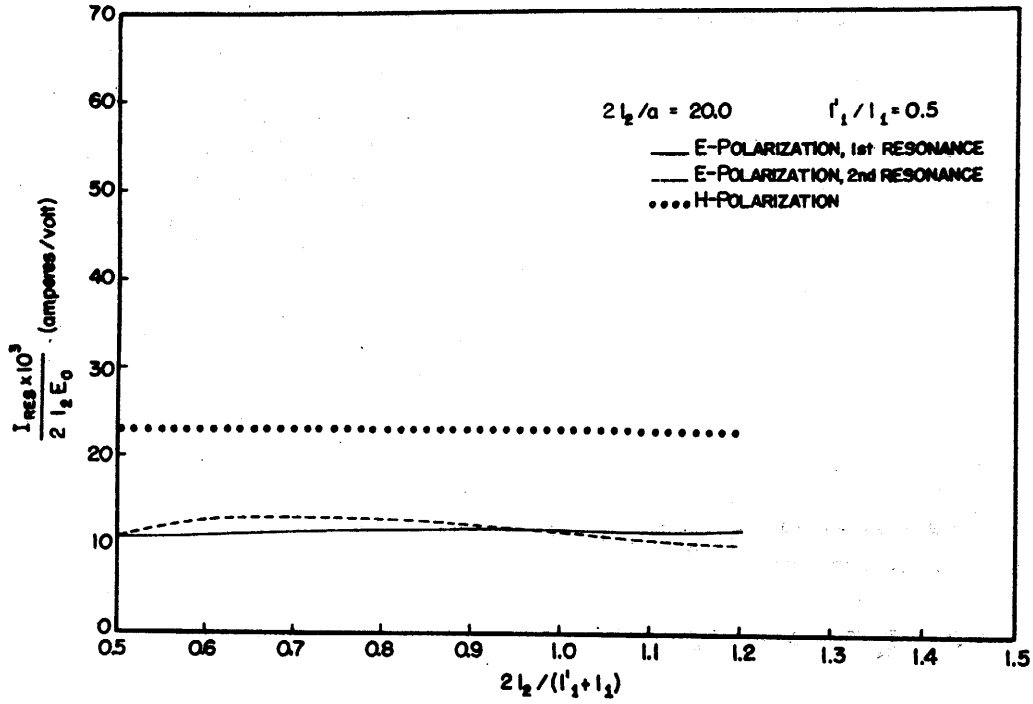

FIGURE 41. Resonant junction currents on wire 2 vs $2l_2/(l'_1+l_1)$.

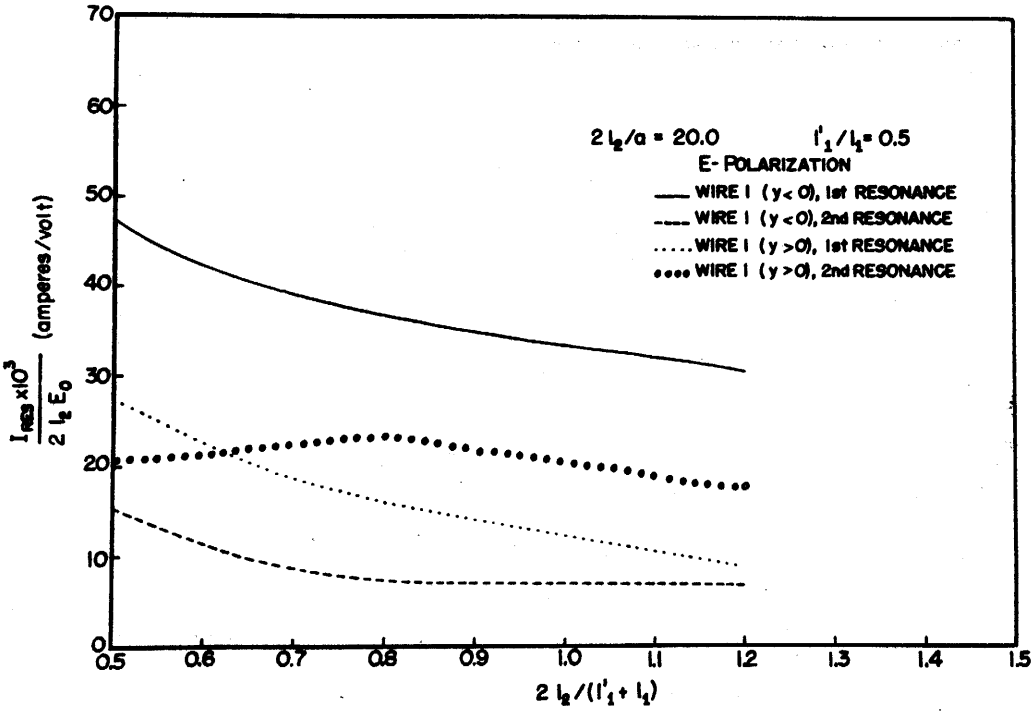

FIGURE 42. Resonant junction currents on wire 1 vs $2l_2/(l'_1+l_1)$.

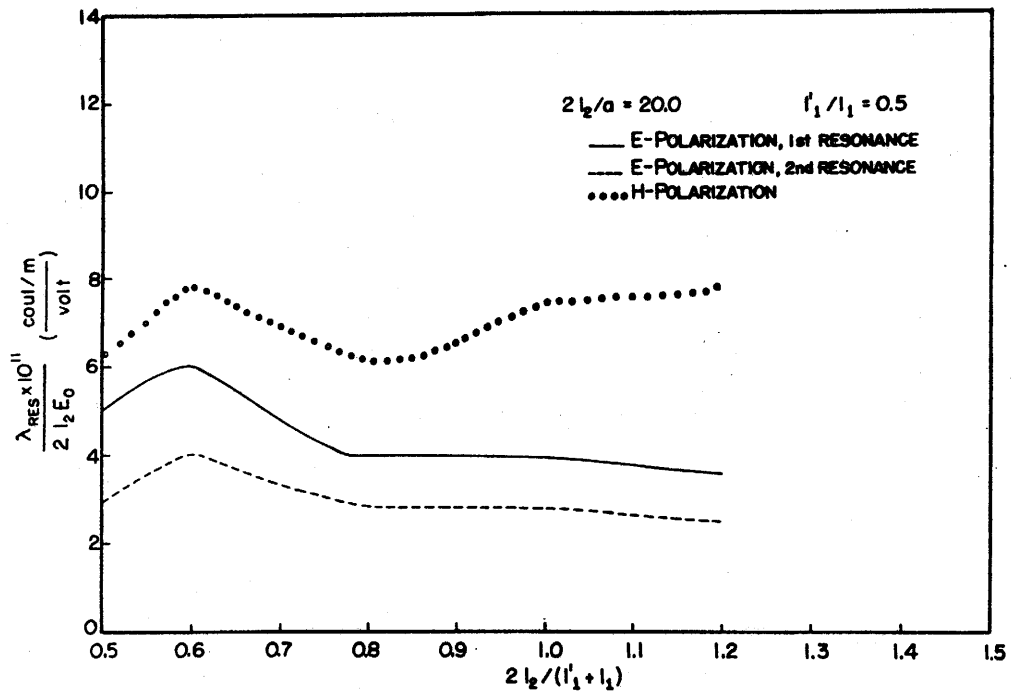

FIGURE 43. Resonant linear charge densities on wire 2 at ~0.7 l_2 vs $2l_2/(l'_1+l_1)$.

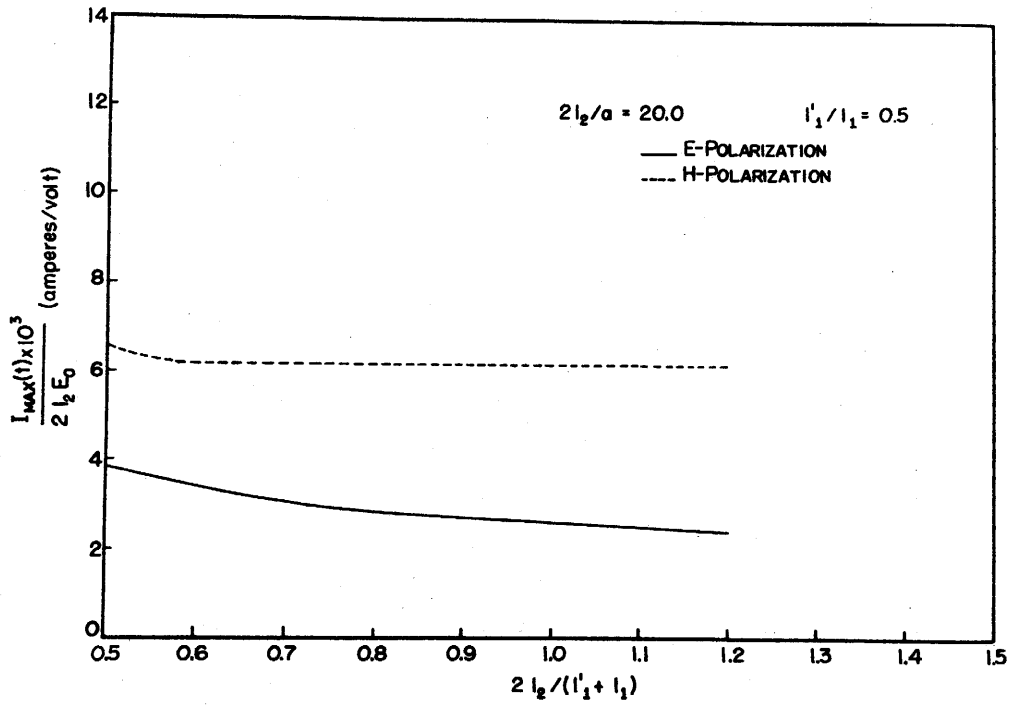

FIGURE 44. Maximum junction currents in time on wire 2 vs $2l_2/(l'_1+l_1)$.

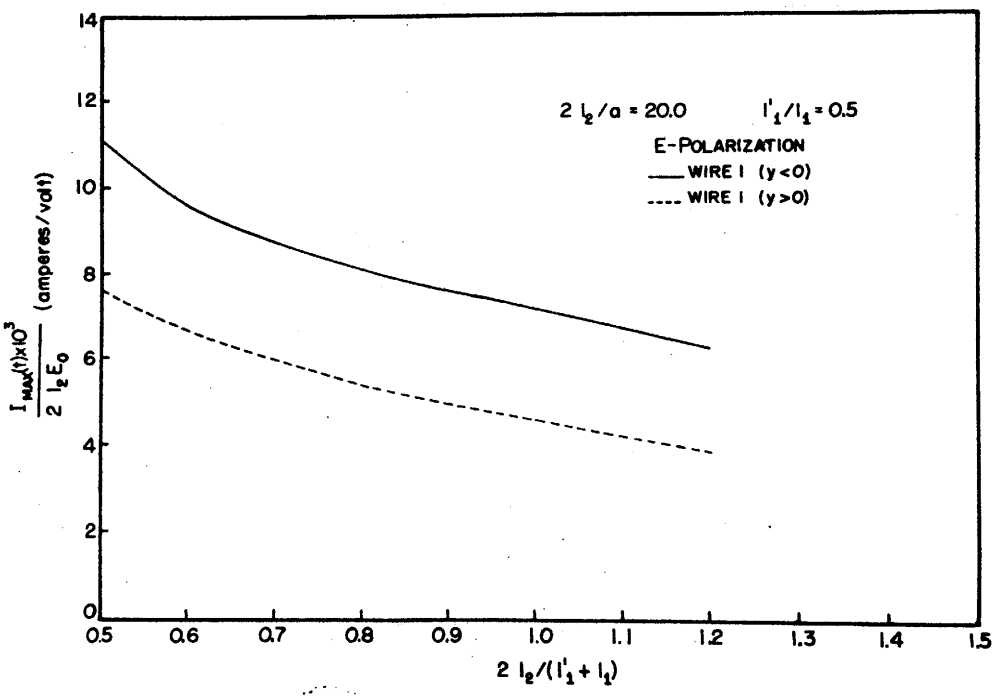

FIGURE 45. Maximum junction currents in time on wire 1 vs $2l_2/(l_1'+l_1)$.

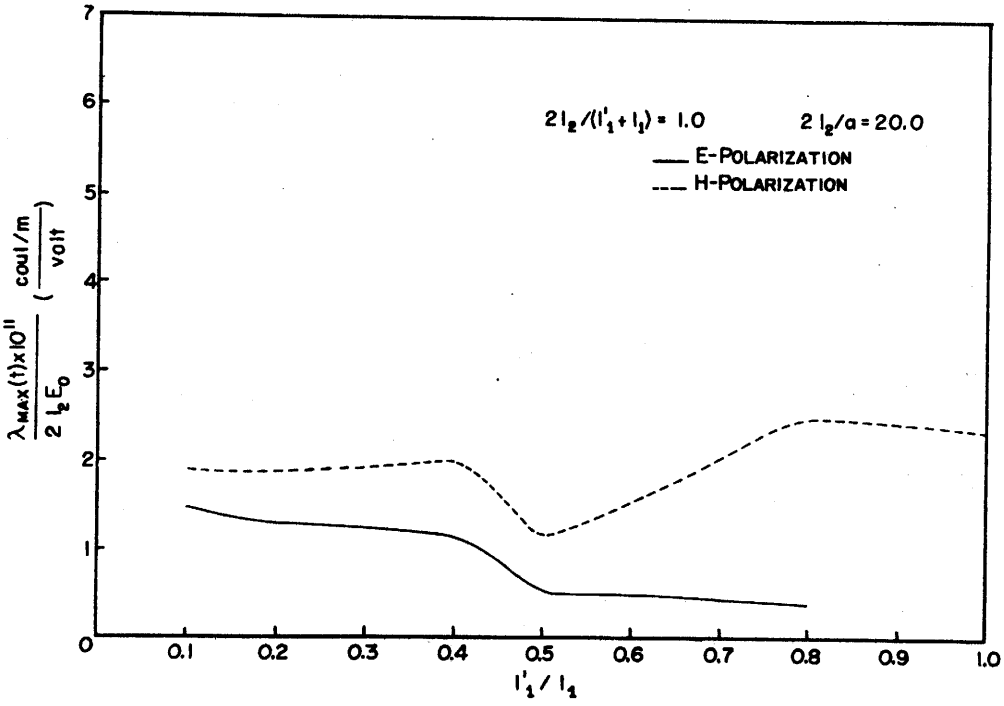

FIGURE 46. Maximum linear charge densities in time on wire 2 at ~0.7 l_2 vs l_1'/l_1.

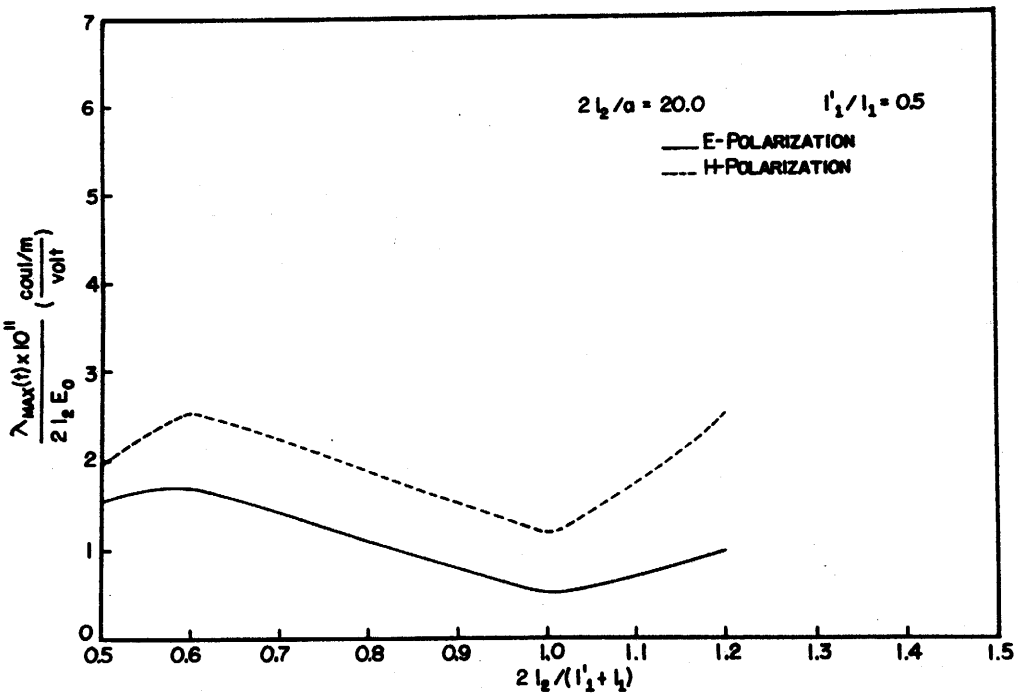

FIGURE 47. Maximum linear charge densities in time on wire 2 at ~0.7 l_2 vs $2l_2/(l_1'+l_1)$.

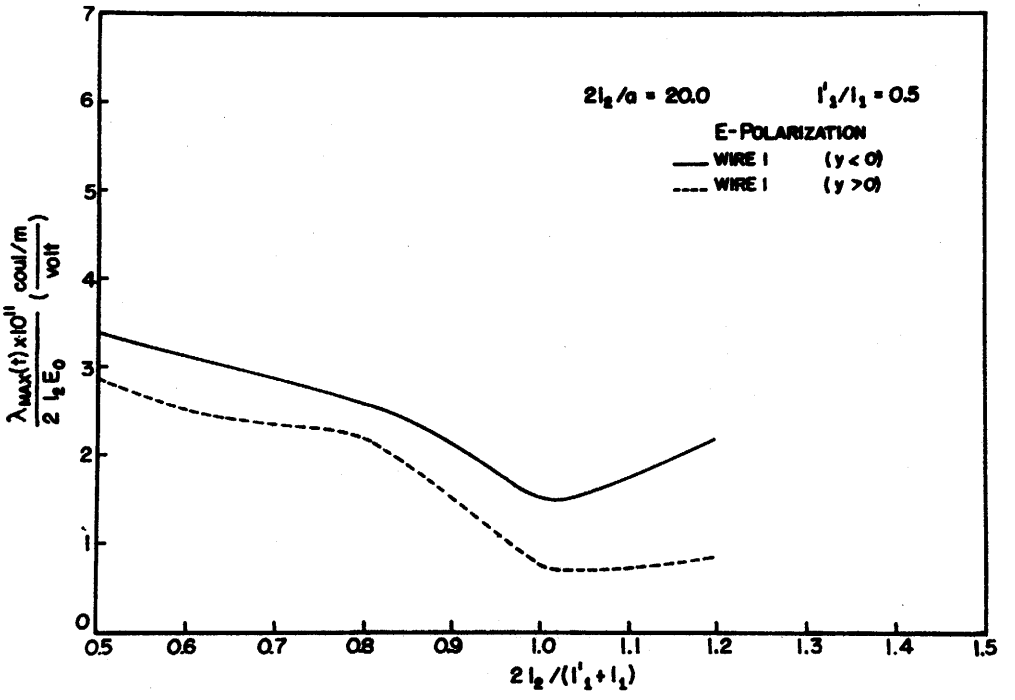

FIGURE 48. Maximum linear charge densities in time on wire 1 at ~0.7 l_1 and ~0.7 l_1' vs $2l_2/(l_1'+l_1)$.

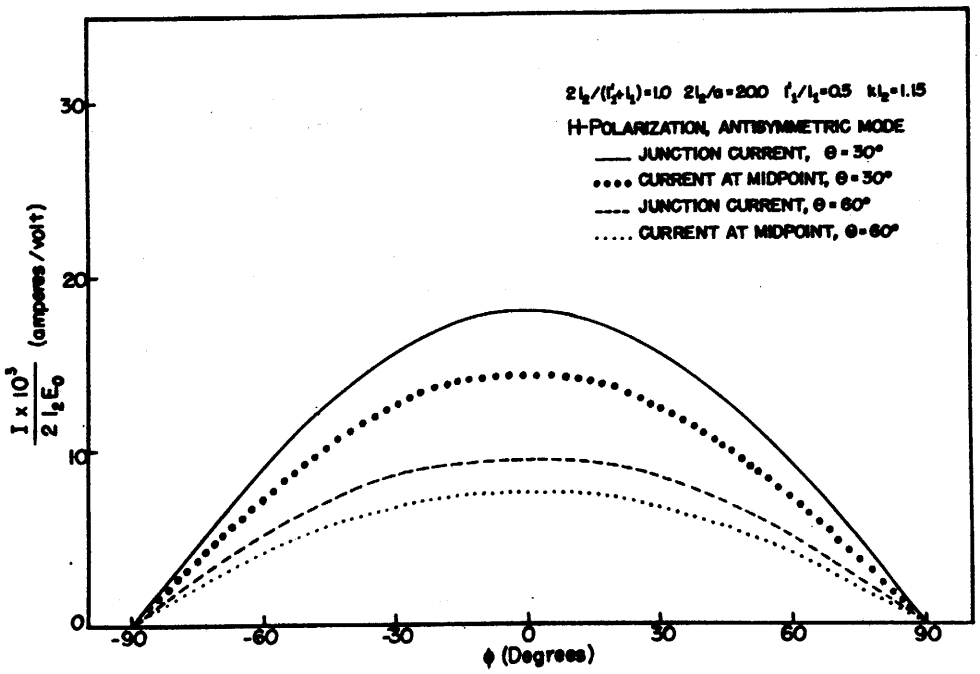

FIGURE 49. Currents on wire 2 vs angle of incidence, ϕ.

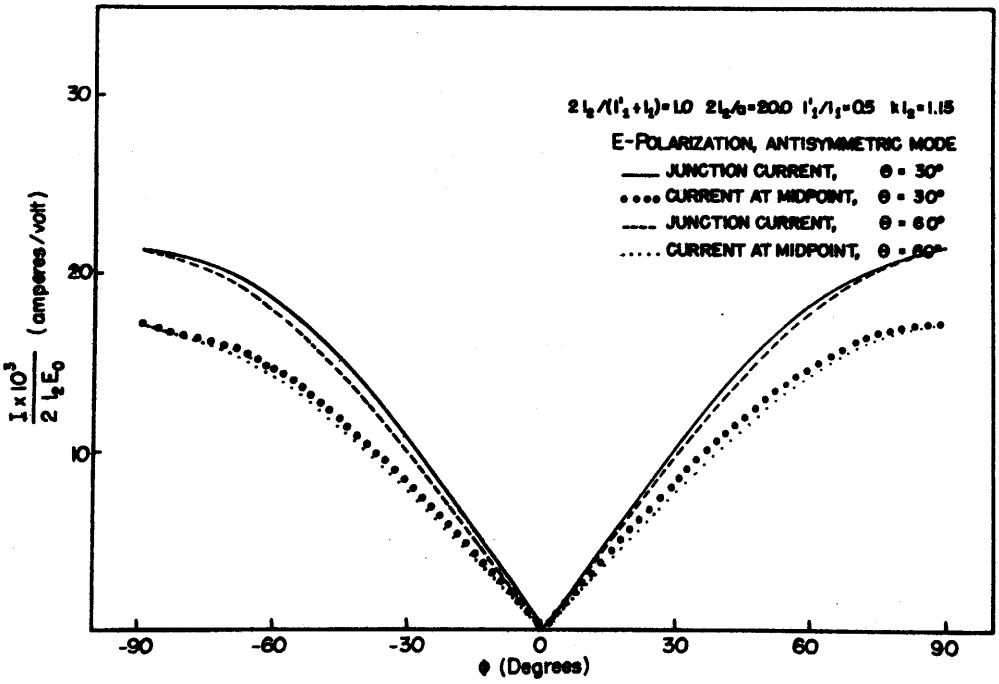

FIGURE 50. Currents on wire 2 vs angle of incidence, ϕ.

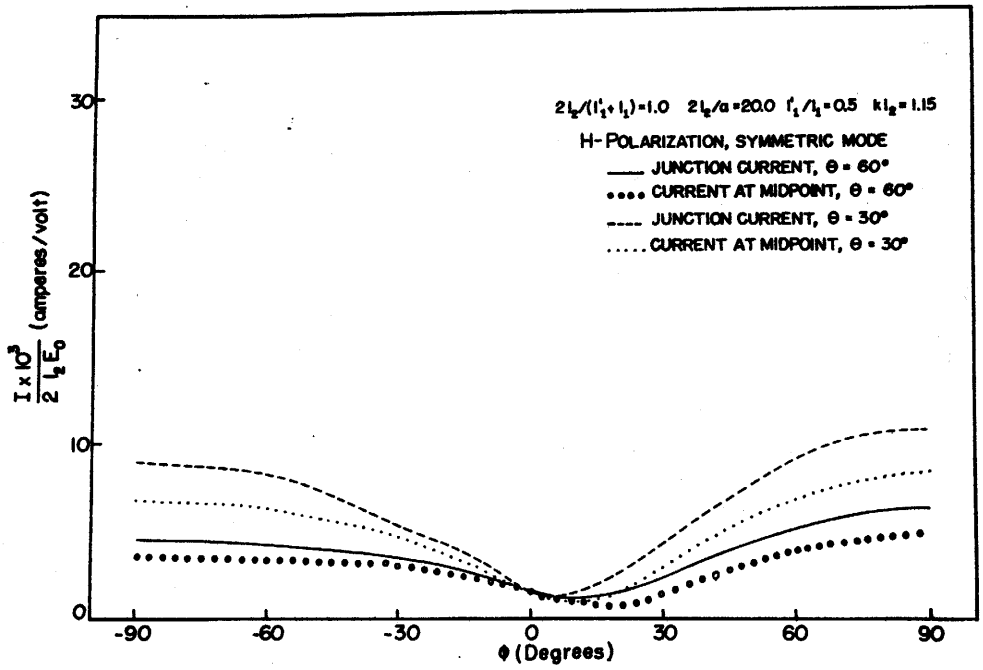

FIGURE 51. Currents on wire 2 vs angle of incidence, ϕ.

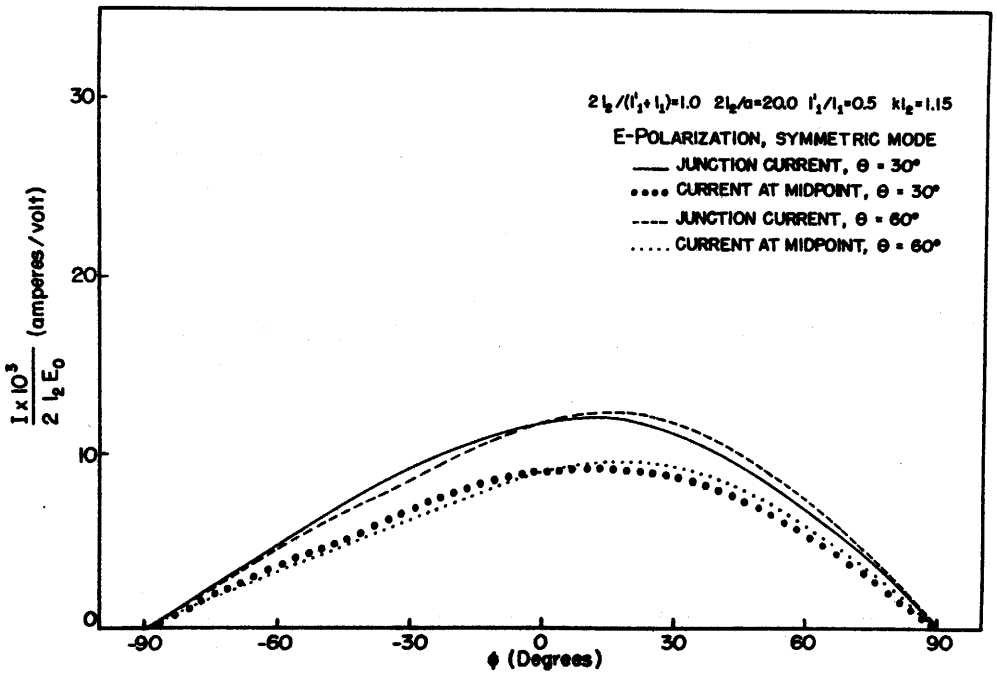

FIGURE 52. Currents on wire 2 vs angle of incidence, ϕ.

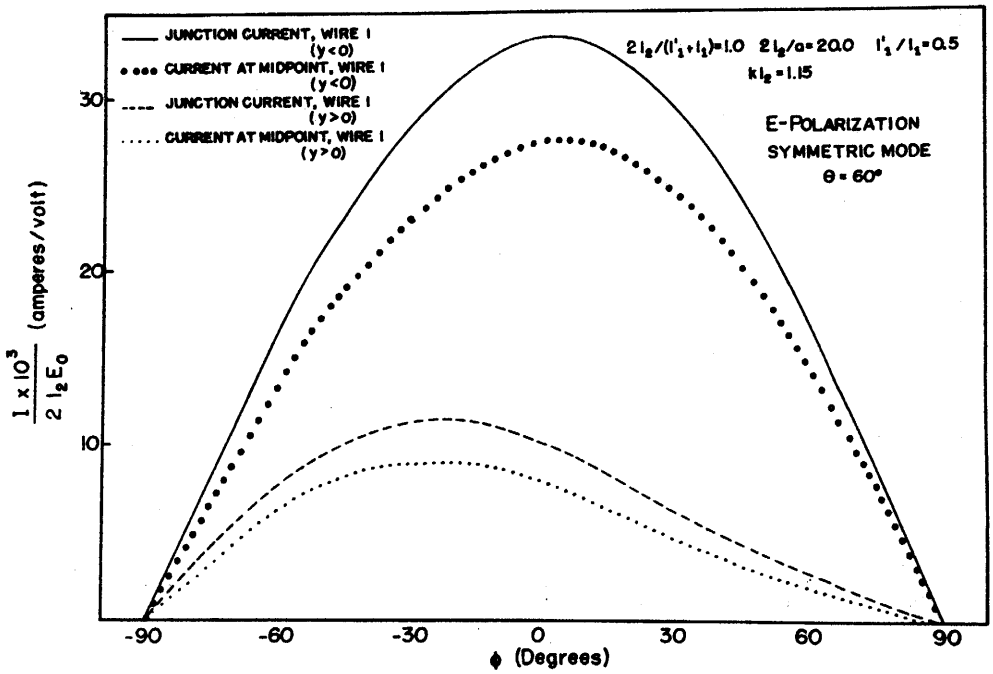

FIGURE 53. Currents on wire 1 vs angle of incidence, ϕ.

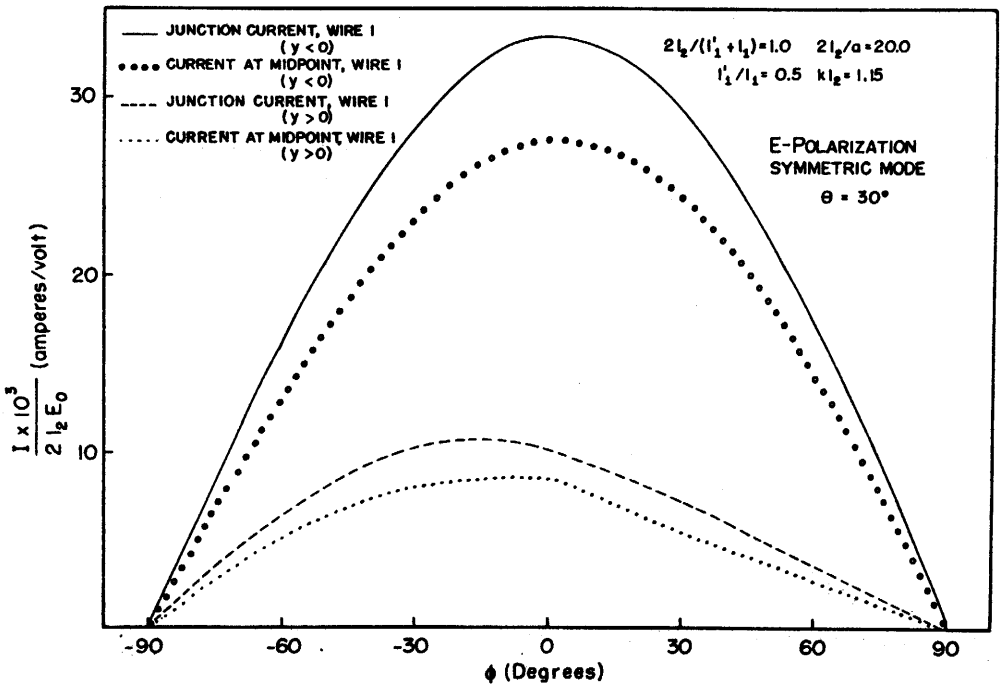

FIGURE 54. Currents on wire 1 vs angle of incidence, ϕ.

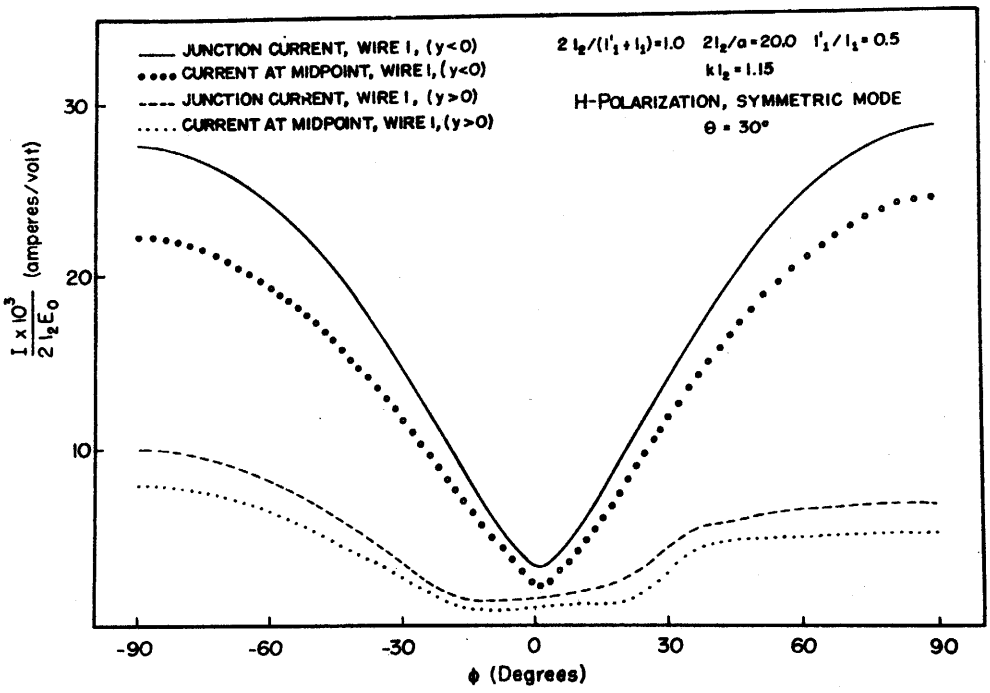

FIGURE 55. Currents on wire 1 vs angle of incidence, ϕ.

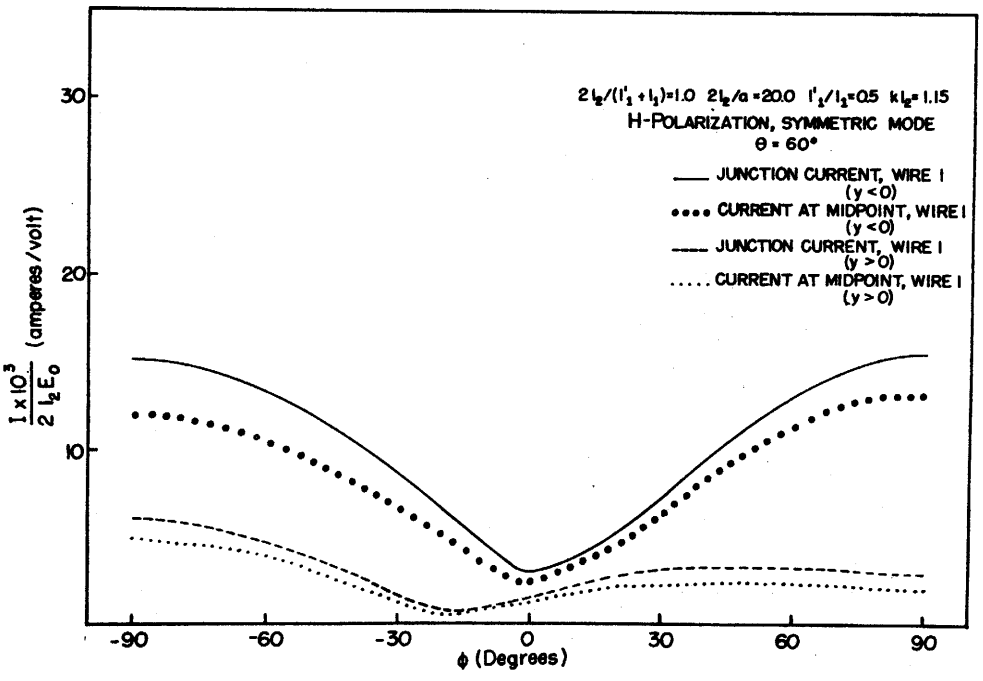

FIGURE 56. Currents on wire 1 vs angle of incidence, ϕ.

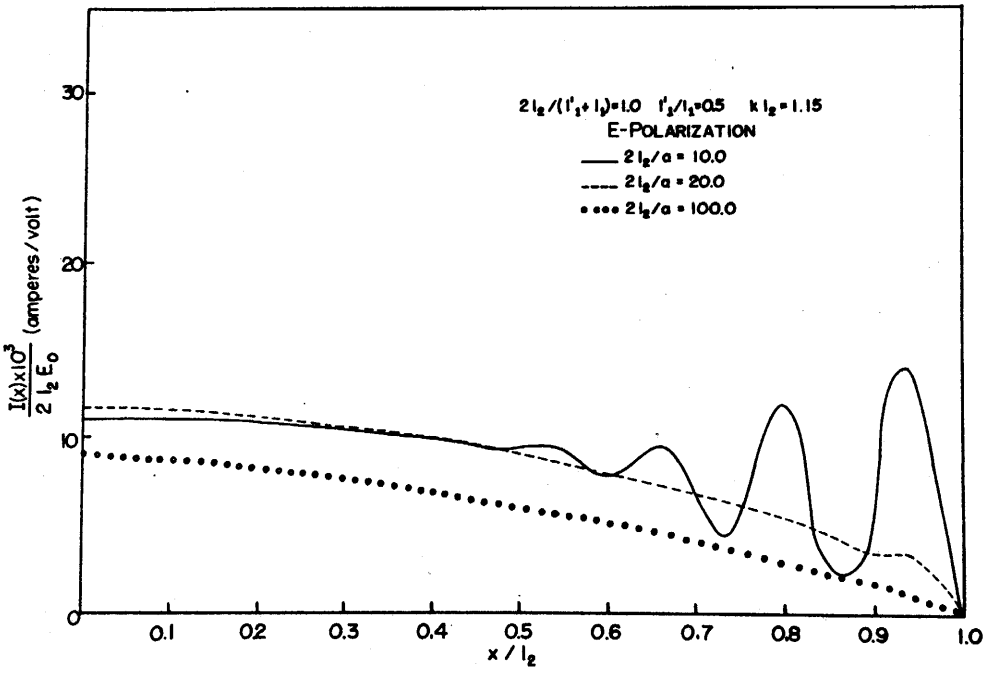

FIGURE 57. Currents on wire 2 vs x/l_2.

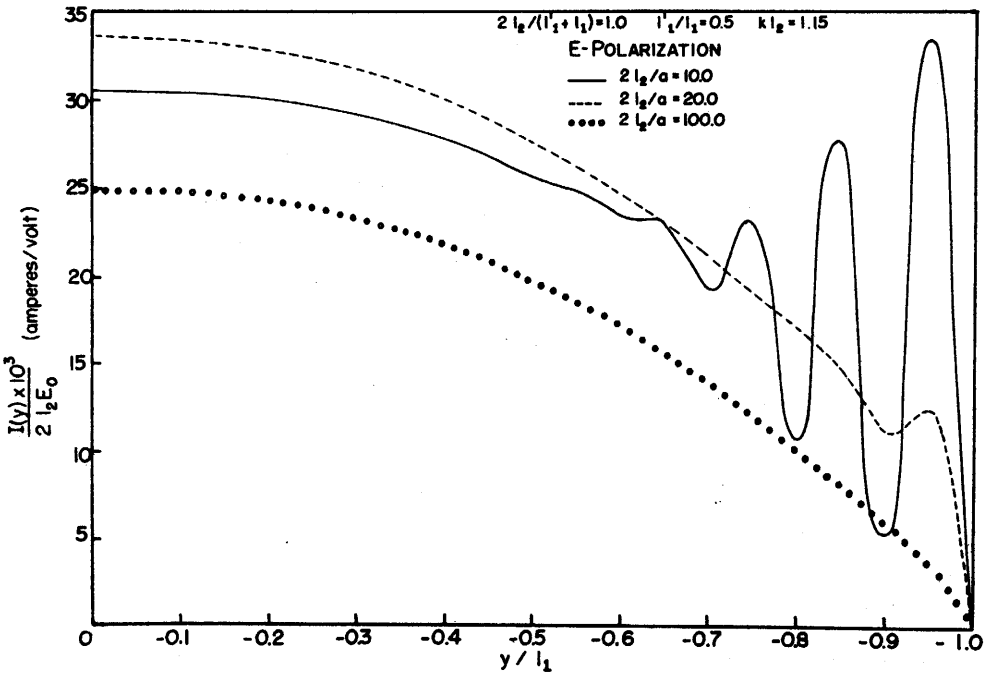

FIGURE 58. Currents on wire 1 (y<0) vs y/l_1.

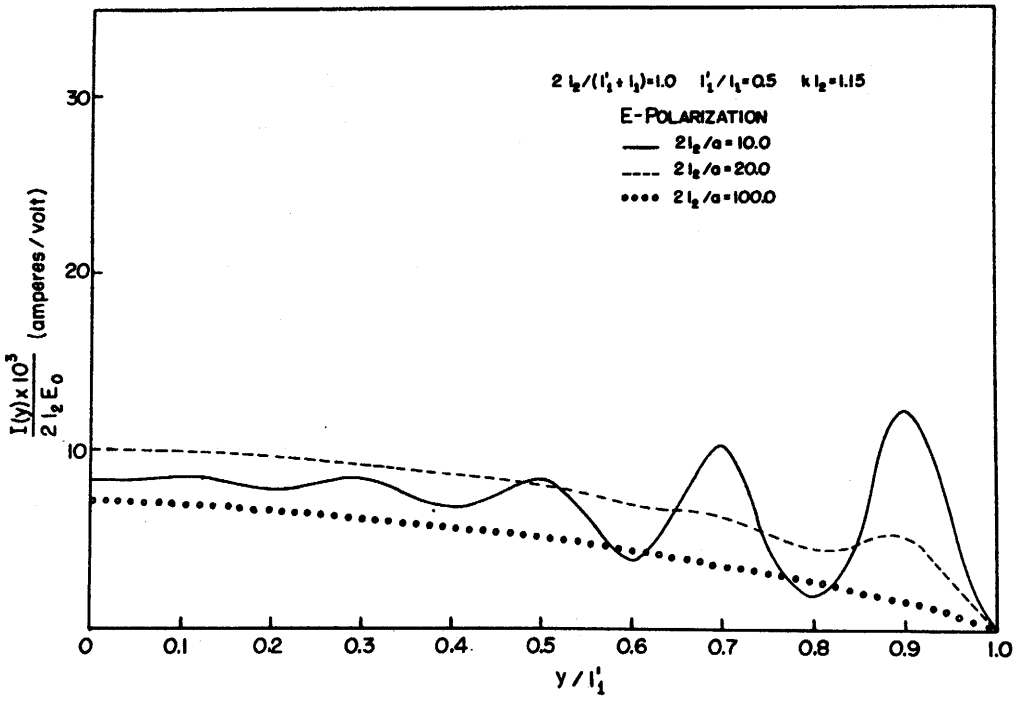

FIGURE 59. Currents on wire 1 (y>0) vs $y/1_1'$.

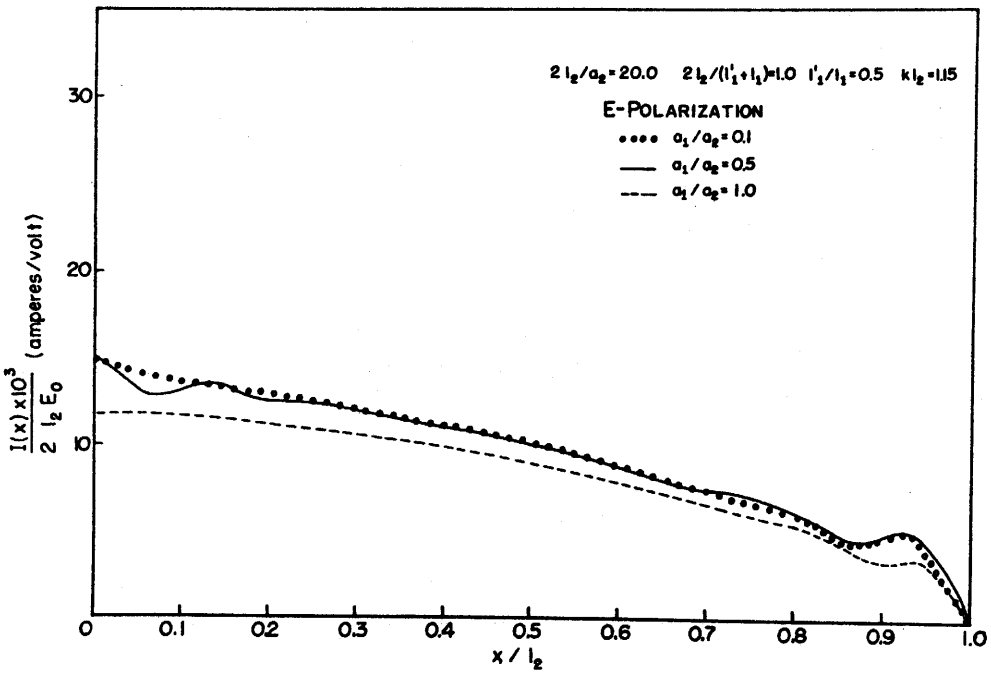

FIGURE 60. Currents on wire 2 vs $x/1_2$.

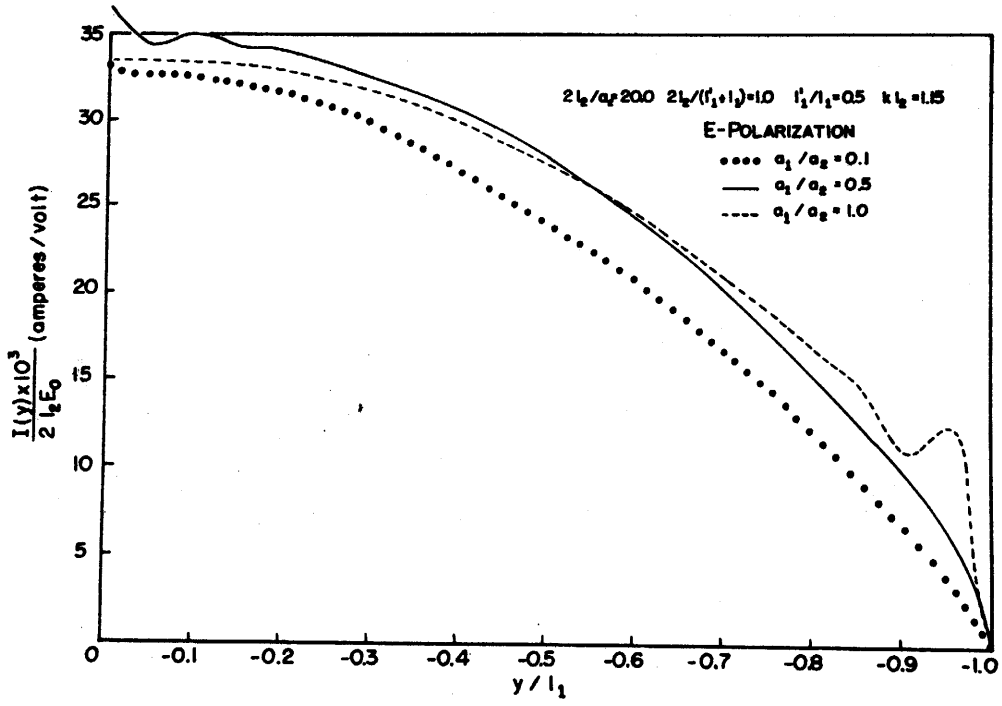

FIGURE 61. Currents on wire 1 (y<0) vs $y/1_1$.

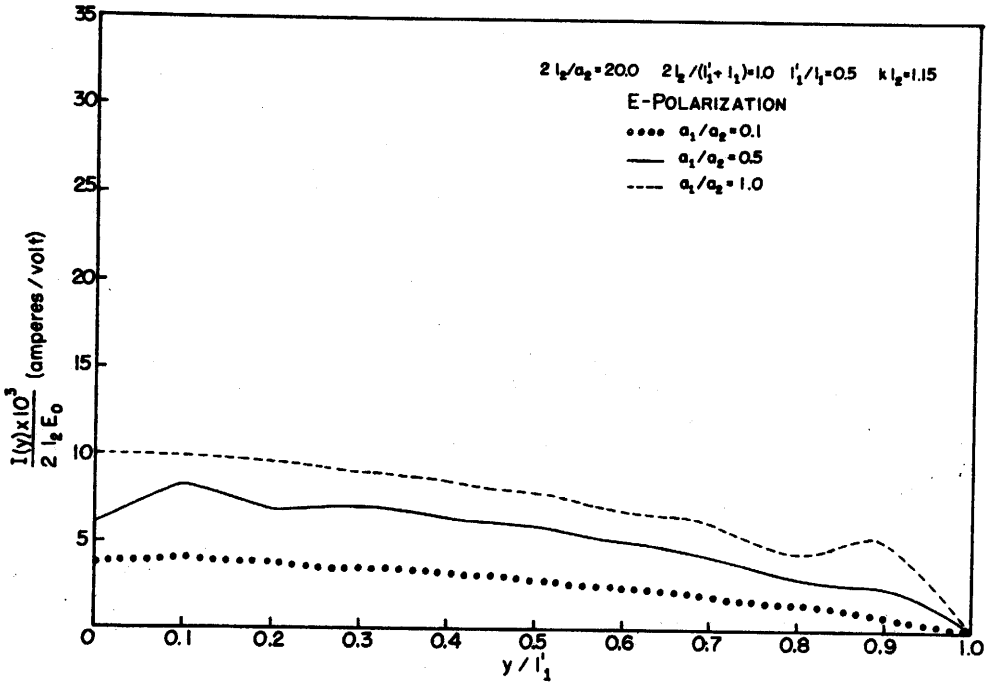

FIGURE 62. Currents on wire 1 (y>0) vs $y/1'_1$.